OPERA 3 - WP1.4b

Project E-NradTech"*Evaluation of New Radar Technologies*"

Subproject 1: *Operational monitoring and use of polarimetric C and S-band radars*

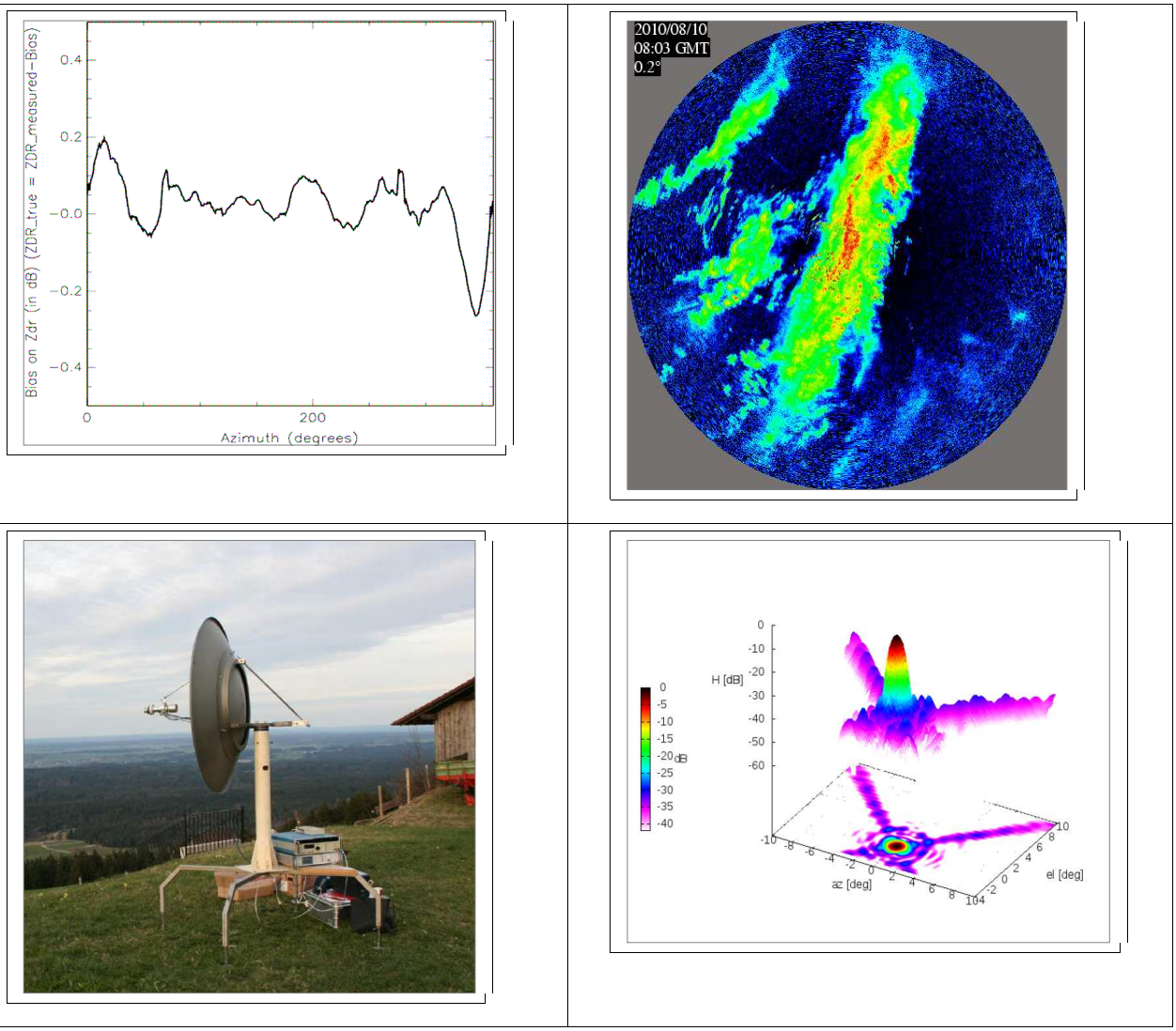

Leader: Météo-France

Contributors: UK Met Office, DWD, ARPA Emilia Romagna

March 2012

OPERA-3 Deliverable Number: OPERA_2012_03

Project Summary

General Informations	
Project Title	**E-NRadTech**
Acronym	**E**valuation of **N**ew **Rad**ar **Tech**nologies
Starting Date	1-Jan-2010
Duration	24 months
Call Identifier	OPERA3- Project Proposal for WP1.4b_1
Keywords	Polarimetry, Polarimetric Variables Monitoring, Quantitative Precipitation Estimation, Polarimetric Data Processing
Description	This report summarizes the early experiences of several Meteorological Services on the Operational use of polarimetric radar data

Project Team

	Partner	**Acronym**	**Country**	**Reference**
1	Météo France	MF	France	Pierre Tabary Jordi Figueras i Ventura
2	UK Met Office	UKMET	UK	Jacqueline Sugier
3	DWD	DWD	Germany	Michael Frech
4	ARPA Emilia Romagna	ARPA-EMR	Italy	Pier Paolo Alberoni

Table of Contents

1. Introduction

Polarimetric systems are now deployed in most European countries and others are planning to upgrade their network with such capabilities. From the research point of view, there is a consensual agreement on the usefulness of polarimetry and multi parameter radar.

Exchanging experiences and findings within the OPERA community is paramount for optimizing and standardizing the introduction of dual-polarization across Europe. This report provides an overview of the current know-how and practices of several European meteorological services which are introducing operationally polarimetric radars in their networks.

Polarimetric variables provide very useful information on the state of the radar system which can be used for early detection of hardware failure as well as to assess the uncertainty in the measurements. Section two of this report describes the polarimetric variables monitoring practices at Météo France, the UK Met Office and DWD. It also provides a discussion of the long term monitoring of the polarimetric radars of the French radar network. Such results are indicative of the polarimetric radar data quality that can be currently achieved.

Polarimetric data quality is highly dependent on the hardware and in particular of the quality of the antenna and the radome. Ideally, the vertical and horizontal channels of the radar system should have identical antenna diagrams. Section 3 describes the efforts performed by DWD in order to characterize the properties of the antenna and the radome.

Radar data contain information that characterize microphysical processes. However, the measurements are subject to uncertainties due to different error sources, e.g. precipitation-induced attenuation, differences in the vertical profile of reflectivity, clutter and artifacts, etc. Section 4 describes the polarimetric variables processing chain developed by Météo France and currently operational in order to correct for most of these errors.

It has repeatedly been proven in the literature that polarimetry can greatly improve quantitative precipitation estimation, QPE. However the use of polarimetry operationally for QPE is still limited. Section 5 shows the main results of a study of different polarimetric QPE algorithms performed by Météo France using operational data. Conclusions and outlook are discussed in section 6.

2. Data Quality Monitoring Procedures: The UK Met Office, Météo France and DWD Experience

2.1. Polarimetric monitoring indicators at Météo France

Météo France developed an in-house polarimetric variables processing chain. It provides several monitoring variables that are essential indicators of the quality of the radar system and its data.

Daily-averaged ρ_{hv} value in rain. It is calculated from average ρ_{hv} values per elevation angle after the bright band is determined. To be included in the computation, measurements must be below the bright band and have a reflectivity factor between 20 and 40 dBZ. A value of 0.99 is expected.

Daily-averaged azimuth-dependent Φ_{dpo} curve for each elevation and for all elevations put together.

Daily-averaged azimuth-dependent Z_{dr} bias curve for each elevation and for all elevations put together. This is calculated from the median of rain-classified gates with Z_h value between 20 and 22 dBZ, where the expected Z_{dr} value is 0.2 dB (see Tabary et al., 2011). Several constraints are imposed (regarding attenuation, ρ_{hv}, number of valid points etc.) to minimize the uncertainty of the measurement.

Daily-averaged Z_{dr} bias at 90° elevation in precipitation. A 90° scan every 15' is included in the scanning strategy of all Météo France polarimetric radars. The expected value is 0 dB. This value is obtained from the median of the range gates between 2 and 6 km which can be assumed to be precipitation. At the end of each day the weighted average of all the valid 90° elevation scans is calculated.

Solar monitoring variables following the method described in Holleman et al. (2010). The method provides the daily azimuth and elevation antenna position biases with respect to the theoretical sun position, as well as the daily receiver Z_{dr} bias and the average sun power P_{sun} for horizontal polarization.

2.2. Polarimetric monitoring indicators at the UK Met Office

The UK Met Office has proposed several procedures to monitor the dual polarization data quality of operational weather radar.

Noise measurement. The noise measured from areas with no reflectivity should be constant and small. This gives a measure of the receiver sensitivity. This test can be carried

out continuously except during wide-spread rain event. Cyclops (Met Office digital receiver/signal processor) produces a long range noise and standard deviation for each ray which is well suited to this task. This information can be used to build a histogram of reflectivity in dB without the range correction for each scan. The noise is expected as a peak in the region of -90 dBm to -110 dBm. The parameters of a Gaussian curve fitted to this peak are used to characterise the noise.

Antenna pointing monitoring with sun observations. Observations of the sun can be used to check the azimuth calibration of the radar. Such observations may be made at sunrise and sunset when the sun is near the scan elevation (within 10° of the horizon). However, rain in the same direction of the sun can invalidate the observations, so most results are achieved only under dry conditions. The present sun spike identifications is based on the final 10% of data in each scan. Cyclops also sends back the long range noise, which would be better suited for this work. A sun spike, when detected, should be at its theoretical azimuth. Therefore, the azimuthal error should be constant and small.

ρ_{hv} value in rain. The co-polar correlation coefficient ρ_{hv} is ideally 1 and the modal value should be above 0.99 in practise. The modal value of ρ_{hv} can be linked to the accuracy of Z_{dr} and Φ_{dp}. Histograms of ρ_{hv} are used to extract and monitor the mode and the spread. The mode should be close to 1, and in any case above 0.99, and the spread should be small.

Z_{dr} bias at 90° elevation in precipitation. At vertical elevation the targets should appear circular, and Z_{dr} should be zero. If this is not the case, the calibration between the two channels must be wrong. Average the reflectivity from a vertically pointing scan across all azimuths. Any slight asymmetry in the targets will cancel out in the averaging process. The result should be constant and small. Any offset is due to channel calibration problems.

Receiver Z_{dr} bias estimation using the sun. Data collected near sunrise or sunset should show a sun spike. Z_{dr} should be zero in the sun spike. Monitoring this allows for the calibration of the receiver path to be checked independently from the transmit path. The present sun spike identification routine is based on the furthest 10% of the scan. Cyclops provides a long range noise field in the ray headers which is suitable for detecting and processing sun spikes. Statistics of Z_{dr} in pixels belonging to a sunspike are compiled from the entire range of the scan. Z_{dr} measured from these pixels should be zero. Any deviation indicates a problem in the radar receive path.

Azimuth-dependent Z_{dr} bias curve for each elevation The differential reflectivity Z_{dr} should be constant across all azimuths. Azimuthal trends in Z_{dr} should be compensated for, and may be due to beam blockages, clutter or radome attenuation. The accumulation of

statistics (mean and standard deviation) of Z_{dr} as a function of azimuth can be used to monitor spectral properties. While Z_{dr} will in general not be zero, by restricting it to a small range of reflectivity (i.e. 20-22dBZ) it should be constant and not show any azimuthal trends. This test requires widespread light to moderate rain over a long time period.

Φ_{dpo} bias The initial phase Φ_{dpo} should be constant. This value is used to correct the differential phase Φ_{dp} , which may be used for calibration of the reflectivity. It is possible that long term variation in Φ_{dpo} might be due to mechanical effects, for example seasonal temperature changes could cause a slight change in Φ_{dpo} due to differential expansion between the channels. These effect are monitored through the averaging of the mean and standard deviation of Φ_{dpo} across all azimuths in vertically pointing scans. Variations in azimuth could be attributed to anisotropy in the radome or by clutter and would have to be accounted for in calibrating Φ_{dp}.

LDR system limit The LDR system limit is a measure of the channel isolation, and ideally should be as low as possible (at least < -35 dB). Simultaneous transmission assumes that both channels are perfectly isolated, and if this is not the case then biases may occur in Z_{dr}.

2.3. Long Term Monitoring Results of the Météo France radar network

Horizontal reflectivity (Z_h)

A procedure to calibrate the horizontal reflectivity of French polarimetric radars using the polarimetric consistency relationship (Gourley et al. 2009) has not yet been introduced into operations at Météo France. Two techniques are currently used to monitor the stability and calibration of the radar horizontal reflectivities: electronic calibration and monthly radar – rain gauge comparisons. Recent work has also been conducted to include results of sun monitoring (Holleman et al. 2010). The procedure consists of measuring the power received from sun hits (which roughly yields an increase of 5 dB in power above the noise floor) and via a complex model, making a daily estimate of sun power, Z_{dr} bias, and antenna pointing bias.

The receivers of the Météo France radars are electronically calibrated every 72 hours. The calibration is performed by using a single stable reference source of 100 mV that is injected into both the horizontal and vertical channels. This signal should have a particular value given the calibration constant provided by the manufacturer. Any deviation from this value is attributed to changes in the receiver gain, and the calibration constant used to calculate the reflectivity at each channel is adjusted accordingly. It should be noted that the signal is

injected into the receivers only and therefore, variations in the antenna gain, rotary joint losses and transmit/receive tubes (hereafter referred to as T/R tubes) losses are not monitored by this technique.

Figure 1 shows the results of a one year (October 2009 – October 2010) monitoring of the daily average of the solar power superimposed with the results of the electronic calibration for four polarimetric radars that are representative of all behaviours encountered in the network. The blue curves (scale given on the left-hand side of each graph) represent the sun power at horizontal polarization (in dBm) while the red curves (scale on the right-hand side) correspond to the electronic calibration results (in dBZ).

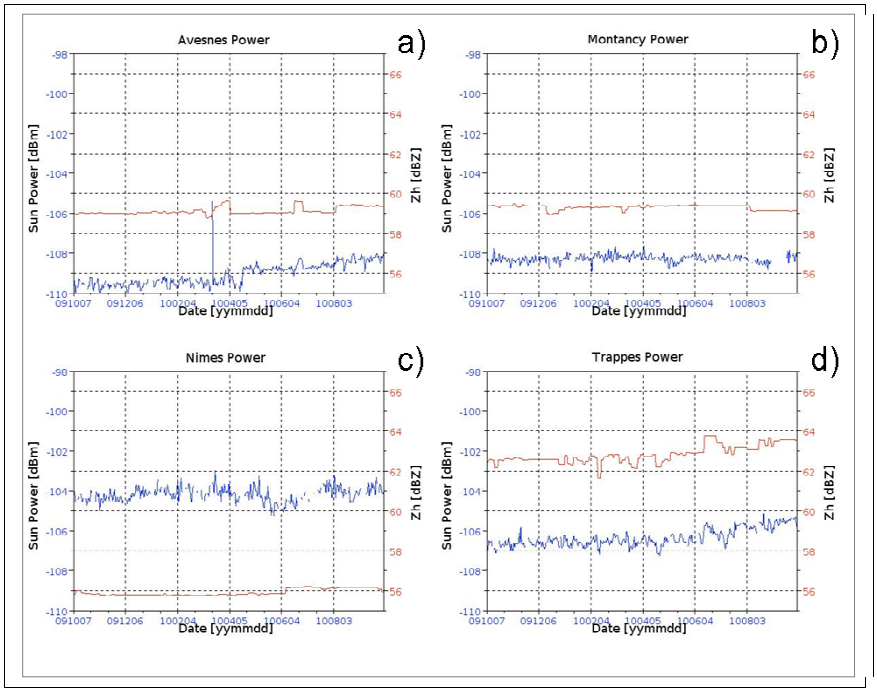

Figure 1 Results of one year monitoring (from 2009-10-07 to 2010-09-30) of the received sun power (blue curve) superposed with the results of the receiver calibration (red curve) of the polarimetric weather radars

To first order, most radars appear to be stable – according to the electronic calibration and sun monitoring indicators - within ±1 dB as the examples of Montancy (Fig. 1b) and Nîmes (Fig. 1c) show. Most radars in the network exhibit a sun power of –108 dBm within ±1 dB. The daily measurement standard deviation is roughly 0.5 dB. There are some exceptions, namely Toulouse, Nîmes (Fig. 1c), and Trappes (Fig. 1d), which exhibit a sun power of –103 dBm, –104 dBm, and –105 dBm respectively. Differences probably result from different waveguide attenuation losses (due to different radar design), different radome types and quality, etc.

An interesting feature of such monitoring is that it provides a useful tool to detect hardware failures rapidly in the radar system. For example, Toulouse (not shown in the graph due to space constraints) suffered from severe degradation of the data which led to a complete stop of operations in March 2010. Investigation showed that one of the flexible waveguides connected to the antenna feeds had broken and water had intruded. These problems were visible in the monitoring data as sudden jumps in the sun power which disappeared after the problem was fixed in May 2010. The correlation between the sun monitoring and the electronic calibration curves is - in some cases – striking. This is for instance the case for Trappes (Fig. 1d), where a regular increase of +1 dB takes place between June and October 2010. Such drift have been found to be very well correlated with changes in the ambient temperature of the radar receiver room. Indeed, Trappes is one of the few radars in the network where the receiver room is not air-conditioned. The jump in sun power in Avesnes the 20th April 2010 is simply an artefact caused by a change in the exploitation mode. Other smaller fluctuations like the ones visible in Montancy do not have a clear origin.

Differential reflectivity (Z_{dr})

There are two elements that may cause a bias on Z_{dr}: 1) the transmission and reception chains, including inaccurate assessment of the losses on each polarimetric channel and 2) the structures close to the radome and/or the radome itself (Sugier and Tabary, 2006). Consequently, the Z_{dr} bias has a potentially azimuth- and elevation-dependent variability that must be compensated.

Holleman et al. (2010) have shown recently that the radar receiver differential bias can be monitored through the sun signatures. Since the sun transmits an un-polarized signal, the expected mean value of Z_{dr} of the sun spike is 0 dB. This may not be the case in periods of intensive solar activity, but evidence of that has not been found in the data. The measurements were rather stable with roughly 0.1 dB daily variance. The differential bias of the entire radar system, including transmission and reception, can be monitored by observing the mean value of Z_{dr} in precipitation when raising the antenna to 90°. In that case, the expected mean value is also 0 dB. The difference between the sun Z_{dr} bias and the 90° Z_{dr} bias can be attributed to the transmitter's bias.

Figure 2 shows the results of a one year (October 2009 – October 2010) monitoring of the Z_{dr} from sun hits (red curves), superimposed with the 90° Z_{dr} bias (blue crosses) and the results of the electronic calibration (grey curve) from some of the radars in the network. The vertical scale spans 10 dB, from -5 dB to +5 dB.

From the comparison between the Z_{dr} 90° curve and the Z_{dr} from sun hits it can be concluded that in general the radars transmitters are fairly stable and that most of the variability on Z_{dr} thus stems from variability of the receivers. In terms of Z_{dr} temporal stability, which is the first requirement to envisage operational quantitative use of Z_{dr}, some radars appear to be quite good (i.e. their Z_{dr} fluctuations, revealed by either the sun monitoring indicator or by Z_{dr} 90°, are less than ±0.2 dB) as shown by the examples of Avesnes (Fig. 2a), Montancy (Fig. 2b), and Nîmes (Fig. 2c). As for the reflectivity curves, the Z_{dr} monitoring provides a good tool for early diagnosis. For example, a T/R tube failure occurred in August 2010 in the Abbeville radar resulted in a sudden increase in Z_{dr} bias (not shown in the graph due to space constraints). The joint and regular increase of the sun Z_{dr} and Z_{dr} 90° of 1 dB over 3 months (June – October 2010) on Trappes (Fig. 2d) is still under investigation. A potential explanation could reside in the temperature of the room where the receivers are located affecting differently the vertical and the horizontal receivers. Overall, Figure 2 is quite encouraging but also shows that there is still some work needed on the calibration and maintenance procedures to achieve a stability of ±0.2 dB on Z_{dr}, which is required to envisage quantitative use of Z_{dr} in real-time operational applications.

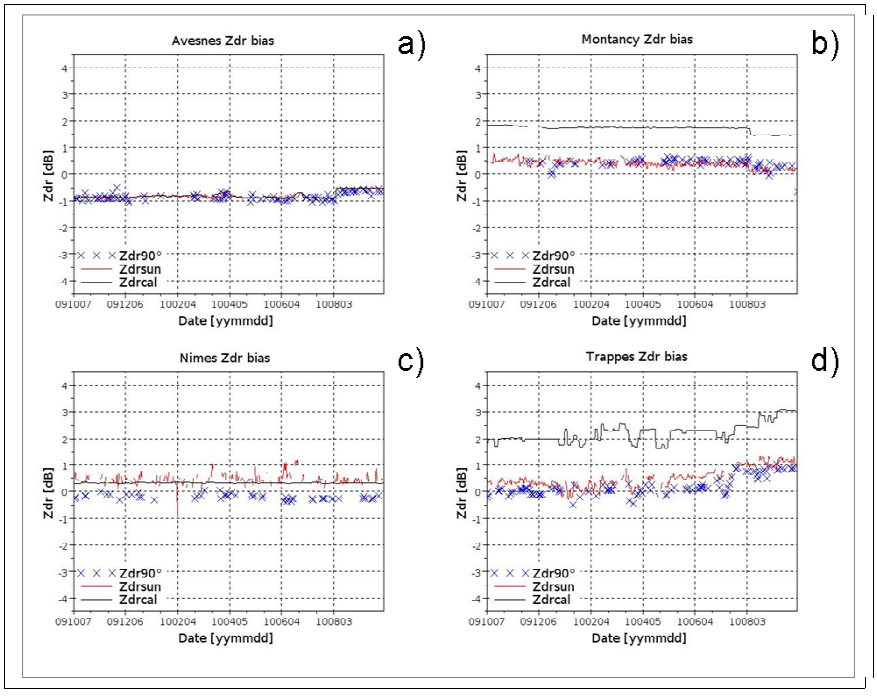

Figure 2 Results of one year monitoring (from 2009-10-07 to 2010-09-30) of the Zdr from sun hits superposed with the 90° elevation Zdr and the results of the receiver calibration of the polarimetric weather radars.

Figure 3 shows the annual monitoring (October 2009 – October 2010) of the azimuth-dependent Z_{dr} bias curves. In ideal conditions such curve should be a flat one with a value of 0.2 dB. What is actually observed is a sinusoidal like variation centred on a value which is in good correlation with the Z_{dr} bias at 90° (see Fig. 2). The form of the curve is attributed primarily to the radome structure (Sugier and Tabary 2006). Indeed, there are three types of radomes in the network, which are distributed as follows:

- Avesnes (Fig. 3a), Blaisy, Cherves, Momuy, Montancy (Fig. 3b) and Montclar;
- Abbeville, Toulouse and Trappes (Fig. 3d);
- Nîmes (Fig. 3c);

Due to the stringent conditions that are imposed, the number of retrieved curves is limited. It varies from 6 curves (Nîmes) to 43 (Trappes). More curves could be obtained by extending the Z_h interval of eligible Z_{dr} values (currently set to [20;22] dBZ, see section 2.2 above) but that would be at the expense of the quality of the Z_{dr} bias estimation.

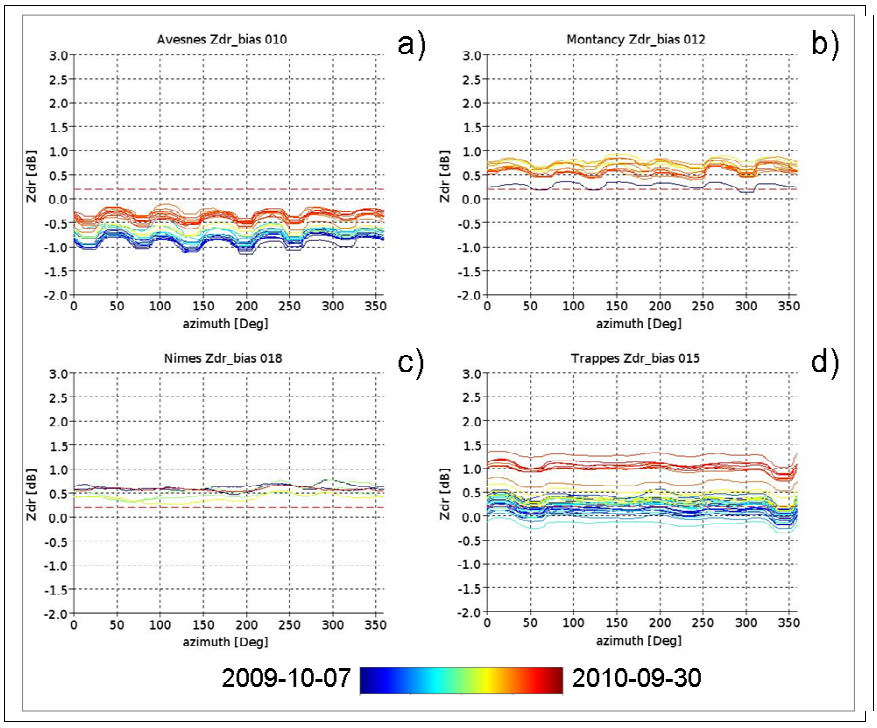

Figure 3 Results of one year monitoring (from 2009-10-07 to 2010-09-30) of the Zdr azimuth bias of the polarimetric weather radars

Phase-based parameters (Φ_{dp} and K_{dp})

An accurate estimation of the system differential phase (Φ_{dpo}) is essential for a good attenuation correction. The attenuation is considered to be directly proportional to Φ_{dp} and therefore errors in the correction of Φ_{dpo} result in under- or over-estimations of the path-

integrated attenuation (and differential attenuation). As for Z_{dr}, it has been shown (e.g. Gourley et al. 2006) that Φ_{dpo} may have a dependency with azimuth either because of the radome or because of rotary joints. After several years of operations, it also appears that Φ_{dpo} may experience drifts or abrupt changes (e.g. following the replacement of a wave guide). This is the reason why decision was made in the polarimetric processing chain to estimate the system differential phase ray by ray in real-time (and not to use to pre-calculated static value).

Figure 4 shows the evolution of the Φ_{dpo} curve during a one year period (October 2009 – October 2010) for 4 polarimetric radars representative of the network situation. Notice that the vertical scale spans over 70° for all radars. Most Φ_{dpo} curves present a sinusoidal shape with 6 periods, which is the number of radome's panels. The comparison between Figs. 3 and 4 shows that there is a good correlation between the observed temporal drifts on Z_{dr} and Φ_{dpo}. The aforementioned lack of stability of the radar in Toulouse was readily noticeable since the Φ_{dpo} variability of this radar actually spanned around 200°. Some of the retrieved Φ_{dpo} curves, such as some of the curves shown for Trappes (Fig. 4d) are clearly non-physical. The data selection process and the quality control of the retrieved Φ_{dpo} curve will have to be improved in the future to avoid such non-physical retrievals.

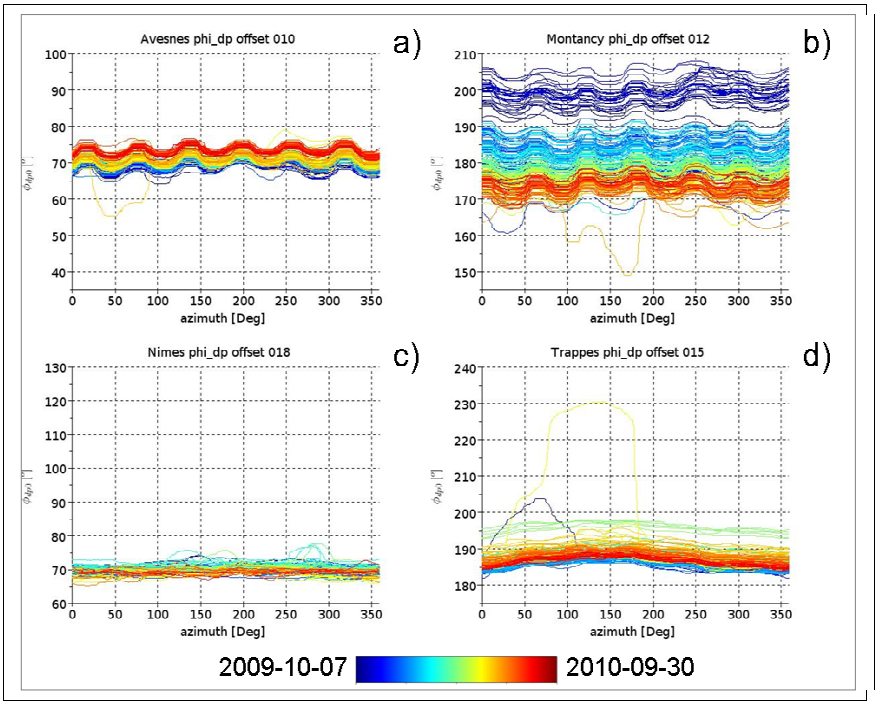

Figure 4 Results of one year monitoring (from 2009-10-07 to 2010-09-30) of the Φdp offset of the polarimetric weather radars.

The topic of K_{dp} estimation has been of interest for several years and various increasingly complex algorithms have been proposed to cope with both the phase noise and δ_{co} (see for example Hubbert and Bringi (1995) or Wang and Chandrasekar (2009)). To evaluate qualitatively the impact of the length of the filter in our simple algorithm, a numerical model was developed. In this model, rain cells are characterized as having a Gaussian shape profile along range. The expected K_{dp} at C-band is derived from this rainfall rate profile using the Beard and Chuang equilibrium drop shape distribution. Then Φ_{dp} is obtained by integrating the K_{dp} profile along the path. A Gaussian phase noise with a standard deviation of 3° is added to simulate a realistic Φ_{dp} profile. The K_{dp} estimation methodology is then applied to the resultant profile. In addition, the impact of the quantization of Φ_{dp} and of K_{dp} are considered.

The results show that the error due to quantization are negligible. They also show that the relative error can be on the order of 100% or higher in areas with light rain since in those areas Φ_{dp} is of the same order of magnitude of the phase noise. Narrow precipitation cells are largely underestimated by the estimator. Phase noise may result in negative estimated K_{dp} (and therefore negative rainfall rate estimated). The average absolute error in the estimation of the rainfall rate is on the order of 3 mm/h. When a narrower filter of 13 range gates is applied, narrow precipitation cells are well estimated. However the average absolute error in estimation of the rainfall rate is doubled to 6 mm/h. These results are in good agreement with those previously reported in the literature such as Gorgucci et al. (1999).

The current K_{dp} estimation may be limiting for QPE at short space/time resolution (e.g. 250mx5'). However, for the hourly accumulations evaluated, the fixed filter length of 25 gates seems to be a good compromise between the need to minimize the error due to phase noise and the need to estimate correctly rain cells as narrow as possible. Indeed it will be shown by the comparison with rain gauges that a narrower filter gives worse results than the current operational filter.

2.4. First monitoring results of the DWD radar network

DWD is currrently replacing the radar network with EEC's DWSR5001/SDP/CE radars. In the end of this replacement project a homogeneous (with respect of the radar type) radar network of 18 dual-polarization weather radars will be available. Parallel to the replacement of all old radars a DWD project called "Radarmassnahmen" has been launched mid 2010. The goal of this project is to make use of the new dual polarization systems. Primary focus is the implementation of operational usable QPE and HMC algorithms. The quality of those

algorithms are of course very much dependent on the quality of the basic dualpol moments. So quality control of those moments are an important aspect in this project. DWD's operational maintenance concept foresees that the new systems will be maintained only every 9 months. Therefore monitoring methods which focus on the data quality and the system health become crucial to guarantee a high availability of the systems.

Similar to the methods presented in the previous section methods to monitor the receive and transmit are implemented for the new DWD dualpol systems. Detection and analysis of sun spikes from the operational scanning and the analysis of a calibration scan at 90° elevation are implemented to date in 5 systems and first preliminary results of about 3-4 months of operation of the monitoring are introduced in this section.

Some key aspects of the sun-spike detection implementation

- we also have implemented the methodology following Holleman et al., 2009. Typically 30 sun spikes (season dependent) can be extracted from the operational scanning every day (solely based on the time stamp of the ray). As a radar monent we consider directly the measured SNR in H and V. Those data are analyzed for range bins in the free atmosphere (~ 10 km above the surface). Peak power in dBm are computed for H and V, and the results are used to compute the differential power of for the receive chain of the radar system. This method appears quite robust also for situations with precipitation present.
- Pointing accuracy of the antenna is computed separately in H and V. The difference is used to monitor the beam squint of the antenna. An unacceptable beam squint may result from a feed-misalignment.

Some key aspects of the analysis of the 90° calibration scan

- Sweep averaged Z_{dr} and Φ_{dp} is computed from the calibration scan. The scan is performed at the end of the volume scan. The evaluation is done only for data in the far field (~ > 600 m above the radar site).
- Mainly stable results are found so far. Some temperature dependencies have been found so that a/c of the receiver is an aspect to pay attention to.
- Z_{dr} and Φ_{dp} appear to be insensitive to the hydrometeor type or to the presence of a bright band (Neuhaus example).

An example result from Neuhaus is shown in Figure 5. There we find an overestimate of about 1dBm . Solar power seen by the radar is on the order of 100 dBm.

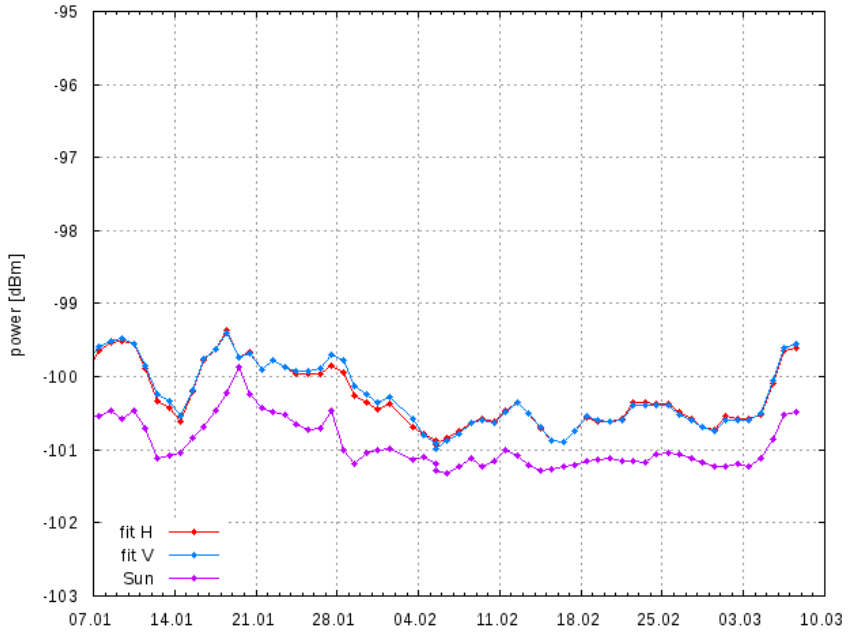

Figure 5: Example from the Neuhaus Radar. The peak solar power seen by the radar compared to solar flux measurements (in dBm). Each data point of the radar power represents the result of the analysis of sun hits from the previous three days. This explains the lag between the sun and radar data.

A typical result from the calibration scan is shown in Figure 6.

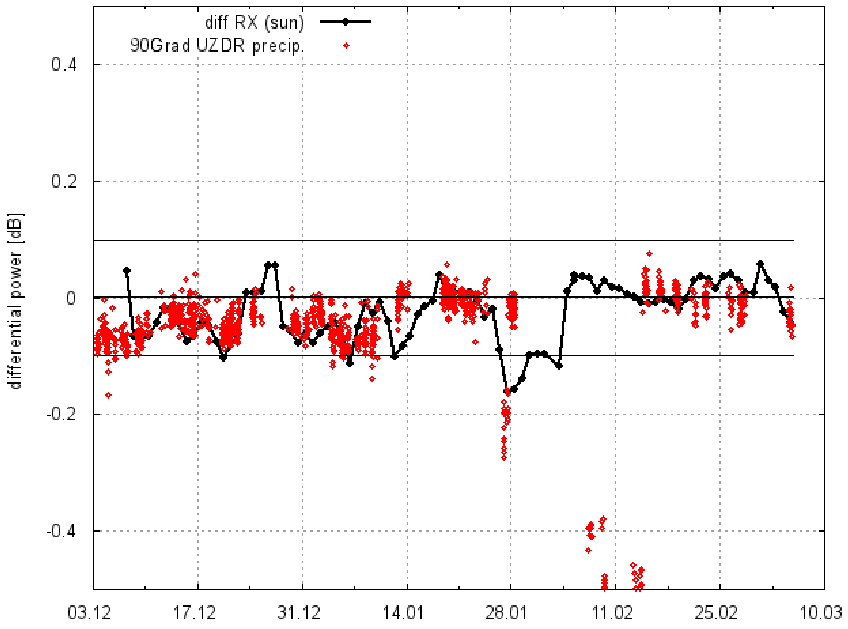

Figure 6: The result from the calibration scan at 90° elevation (8 weeks). Mean Z_{dr} is computed only for RHOHV > 0.9 and a SQI > 0.5. The corresponding RHOHV and SNRh data are shown. The drop in Z_{dr} on 27.1.2012 relates to the failure of the air conditioning (temperature drop by about 20 K). Low Z_{dr} values in the beginning of February are still a matter of investigation. The Z_{dr} offset has been adjusted on 15.2.2012 and is rather stable since then.

The corresponding differential power in Neuhaus based on the calibration scan and the analysis of sunspikes is shown in Figure 6. This is a nice example showing a good match of the receiver path. Note that this plot covers a period of more than 3 months. The corresponding Φ_{dp} is shown in Figure 7. The failure of the a/c caused a ~ 2° change in Φ_{dp}. The Z_{dr} offset at the same time changed by 0.2 dB. The reason for the initial increase in Φ_{dp} around 13.1.2012 is still a matter of investigation.

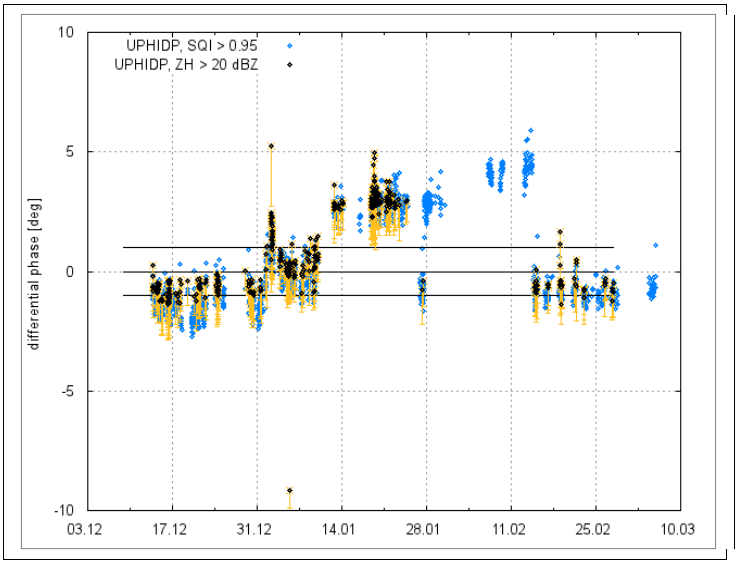

Figure 7: Neuhaus: Differential phase based on the calibration scan at 90° elevation. Two criterion to extract the data are considered. One requires a RHOHV and SQI >0.95, and the other one requires a Z_h > 20 dBZ.

The intercomparison between the radar sites using the sun as a reference suggest an overall bias (overestimate) between 0.5 and 1.5 dB. This is shown in Figure 8. The large bias of the Essen date at the end of this time series is still a matter of investigation. The increasing bias of the Hohenpeissenberg system (MHP) at the end of the time series is related to specific tests that were carried during a training week for DWD's radar technicians.

In addition to the previous mentioned methods we also perform a single-point calibration using the internal test signal generator twice a day.. Result of this have not been analysed in detail so far. A more detailed analysis of the monitoring results is a matter of on-going work. A more generalized view on the new system will emerge with longer time series.

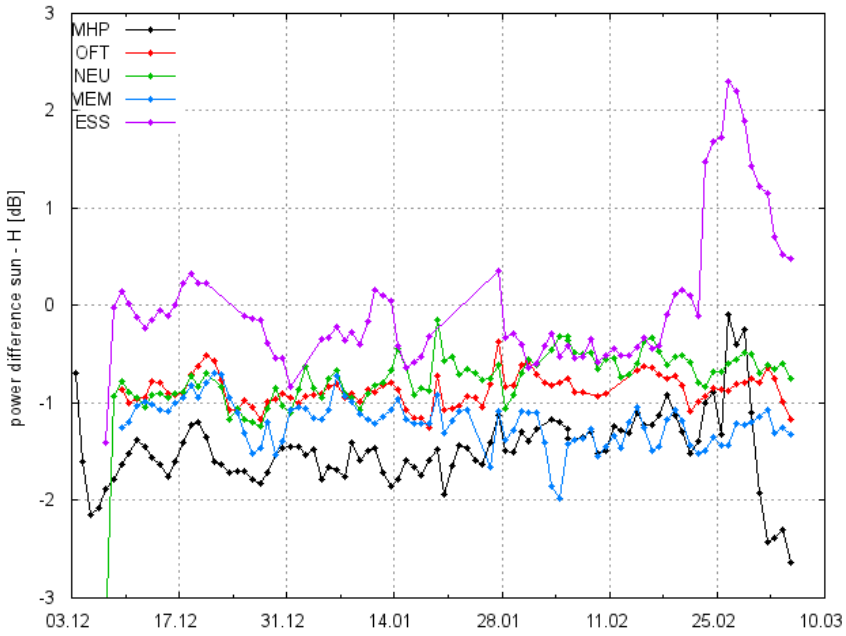

Figure 8: The power differences from sites with the new radar systems. Reference power is the sun. Following sites are shown: ESS = Essen; OFT = Offenthal; NEU = Neuhaus; MEM = Memmingen; MHP = Hohenpeissenberg. The reason for the large excursion of the Essen data the end of February is still under investigation. The Hohenpeissenberg data during that time also shows a large bias there was a technician training. So specific tests were performed so that the operational data during that time is not reliable.

3. Onsite antenna performance verification: measurements with and without radome

3.1. Introduction

The German Meteorological Service DWD is currently replacing all radar systems with new dualpol radar systems using the STAR mode technique (Simultaneous transmit and receive). One of the key components of a radar system is the antenna. For dualpol applications the antenna should have an identical performance in both polarizations meaning that the antenna patterns in both polarizations should match. Commonly the compliance with the specifications of the antenna is proven through antenna patterns which are usually provided by the antenna manufacturer as cuts through the main planes of the antenna including the strut plane. In the course of DWD's acceptance tests of the antenna it appeared that for example the proof of the match between the main beam for both polarizations is limited with the existing equipment on the antenna manufactures test range. In particular the mechanical antenna

pointing accuracy at the antenna manufacturers site appeared not sufficient to show the compliance with specifications. DWD therefore tests the antennas on the radar manufactures test range making use of the capabilities of the new radar system. Those tests are carried out during factory acceptance tests (FAT) for the radar system delivered.

Onsite antenna tests are a unique effort as part of DWD radar replacement project. They have two main goals. One is to prove that the on site antenna assembly procedures guarantee the same antenna performance as shown during FAT. The second aspect is related to the combined performance of the antenna and the radome which in the end determine the operational data quality of the new dualpol radar system.

In an effort to prove parts of the radome performance, dedicated antenna pattern measurements with and without radome were carried out at the Hohenpeissenberg Meteorological Observatory in spring 2011. The installed radome has a random panel design which is optimised for dualpol applications. The design is aiming at electrically seamless RF performance. The layout of the design is based on an impedance matching procedures which includes laboratory measurement of the electromagnetic field due to the scattering effect of the radome panels.

This unique measurement campaign is the first approach to quantify onsite the performance and the effect of a radome on the HF performance of the antenna. The more thorough description of the measurement campaign is documented in Frech et al. (2012). Here we summarize the main aspects and findings.

3.2. Antenna and radome requirements

In the following we summarize the requirements to the antenna and radome HF performance:

Antenna:

Following specifications for the new dualpol antenna where established:

- beam width in H and V (BW) < 1°
- absolute difference of beam with in H and V < 0.03°,
- pointing difference of the H and V beam, the so-called beam squint must be < 0.08°,
- antenna gain in H and V > 45 dBi,
- gain difference in H and V < 0.1 dB,
- side lobes < -30 dB (< +/- 10° off the main beam), < -43 dB (> +/- 10°). The angular distance is relative to the main beam location,

- main beam cross-polar isolation < -32 dB,
- the difference of the power distribution in H and V must be < -5 dB in a range < +/- 10° around the main beam in any angular direction.

Radome:

Following specifications for radome where established:

- one way (dry) attenuation < 0.27 dB.
- Additional beam squint caused by radome < 0.02°.
- the increase of the first side lobe level due to the radome < 0.5 dB
- variation of ZDR (in el and az) < 0.1 dB (radome manufacturer specification: < 0.0005 dB).
- change in Φdp < 1°.
- variation of Φdp (in az and el) <1° (radome manufacturer's specification: < 0.03°).
- difference in one-way attenuation between Zh and Zv < 0.1 dB (radome manufacturer's specification: < 0.005 dB).
- variation of RHOHV (in az and el) < 0.005° for ROHV > 0.99; this means for situations with precipitation).
- variation of LDR (in az and el) < 1.5 dB.

Clearly, the specifications of the radome (in particular in the main beam) and their proof are difficult to achieve, since the numbers are at or beyond the measurement accuracy of the radar system (in particular the radome manufacturers specifications). Plus, there are always some uncertainties related to the test range conditions.

3.3. The measurement setup

The basic approach to obtain an antenna pattern is to place a transmitter at the radar frequency in the far field of the receiving radar antenna. The location of the transmitter has to be chosen such that there are no obstacles in the path. Furthermore, the site has to be selected that minimum scattering at the orography along this path may occur. A favourable source site may be a tall tower or a mountain with e.g. a valley along the transmit path. The onsite antenna pattern measurements are acquired using DWD's radar software package MURAN. During SAT we have chosen three different source sites at three different azimuthal locations. The analysis from all three source sites will be used to assess a possible radome induced azimuthal variability of radar moments.

3.4. Results: Copolar and crosspolar measurement with and without radome

The copolar antenna pattern without radome is shown in Figure 9, and the corresponding copolar pattern with radome is shown in Figure 10. Qualitatively there is an increase in copolar signal strength in some locations to levels above -43 dB, but the difference between the two measurements seems not significant. The corresponding cross-polar power results are shown in Figure 11 (without radome) and Figure 12 (with radome). It is obvious, that the cross-polar levels are increased significantly by the radome. This increase is mainly seen in between the struts up to levels of about -50 dB. There seems to be no significant increase of cross-polar power in the strut plane and in the main beam region. The typical four cross-polar peaks located around the center of the main beam are nicely visible (Zrnic et al., 2010).

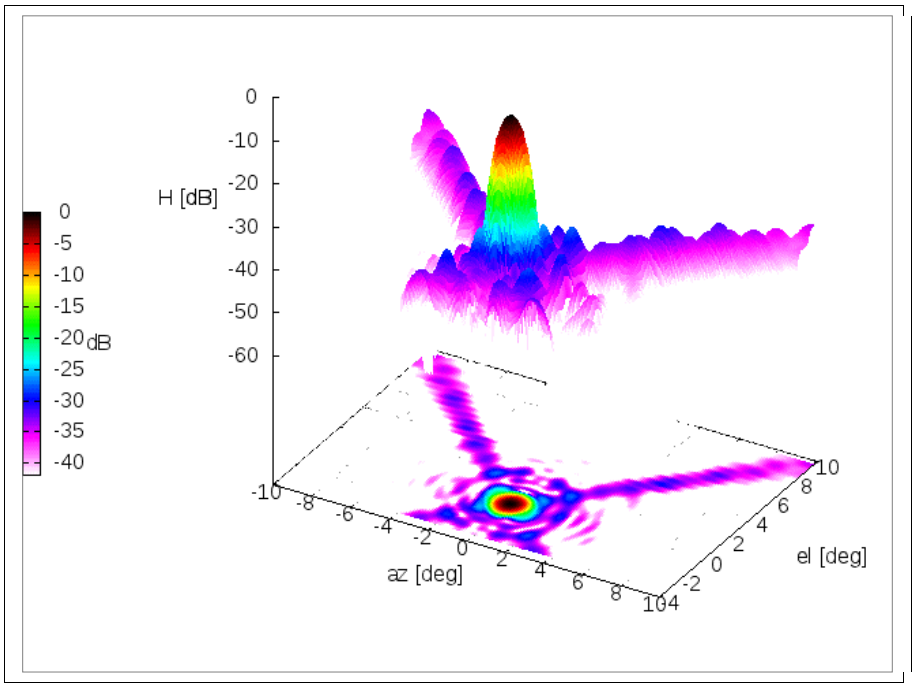

Figure 9: Copolar H plot, source site is a TV tower. Data are taken without radome.

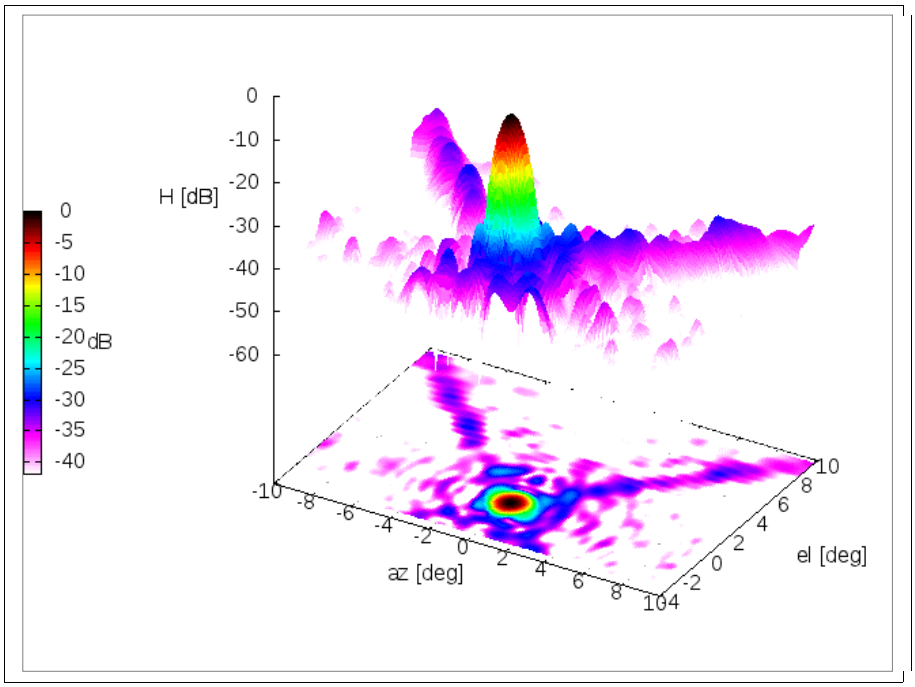

Figure 10: Copolar H plot, source site is the TV tower. Data are taken with radome.

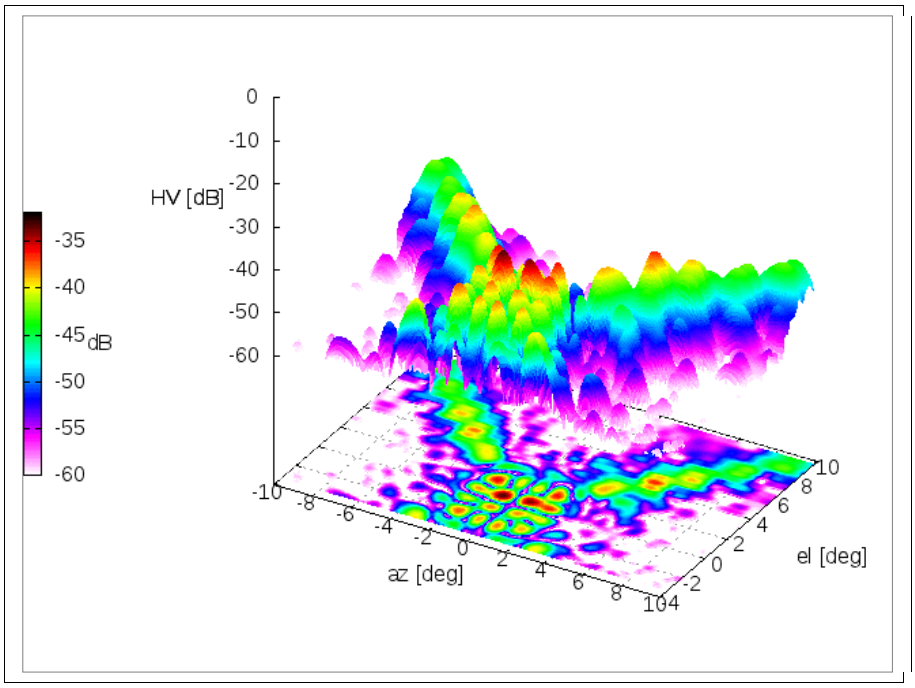

Figure 11: Cross-polar HV plot, source site is the TV tower. Data are taken without radome; HV means transmit in H and receive in V

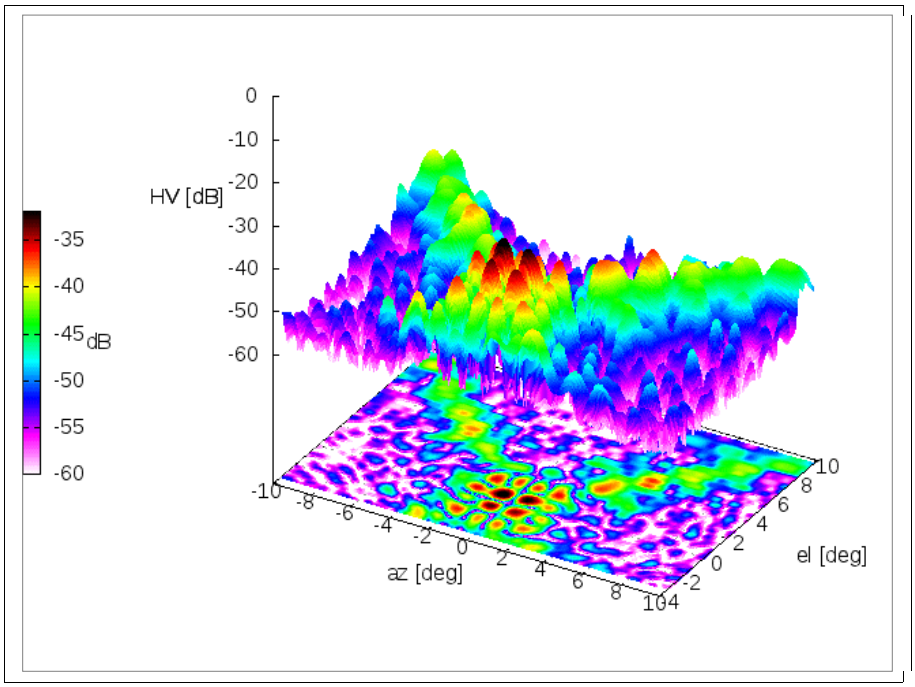

Figure 12: Cross-polar HV plot, source site is the TV tower. Data are taken with the radome in place.

The average copol (H) and cross-pol power (HV) and the corresponding range in the measurements from all three source sites is shown in Figures 13 and 14. There is a significant increase in side lobe levels beyond the first side lobes compared to the measurements without radome. The typical roll-off of the side lobes is not seen and the copolar signals remain on average on a constant level. At some azimuthal positions copolar levels are above the specified -43 dB level From an operational perspective, the levels of the first side lobes are important as they determine the level of clutter echos at low elevations. Based on the specification, the first side lobe must not be increased by 0.5 dB due to the radome. Here in all but one case, this is achieved. In V, we find an increase of 0.9 dB (from -34.3 to -33.4 dB). This might be a measurement artifact, but the large number of measurements and the small variability from measurement to measurement suggest an effect related to the radome. However, the overall performance of the antenna-radome assembly with respect to the influence on the copolar antenna pattern in the main beam area is still very good. The main beams match within less than ~ 1 dB down to -30 dB for a given polarization state (see also below).

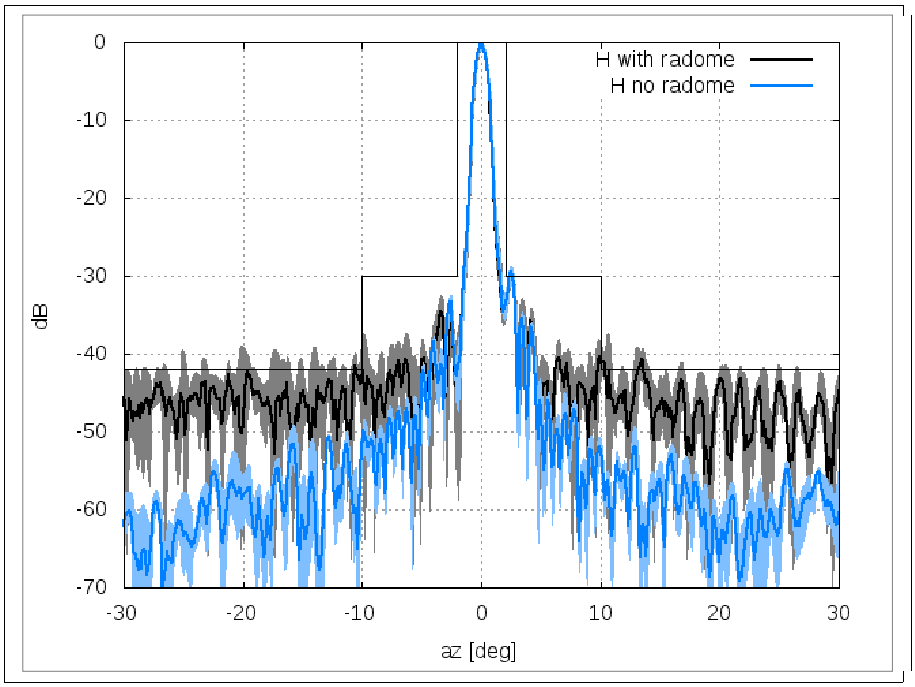

Figure 13: Variability (quartiles) of copolar power H with and without radome in the main plane. Shown are also the antenna specifications.

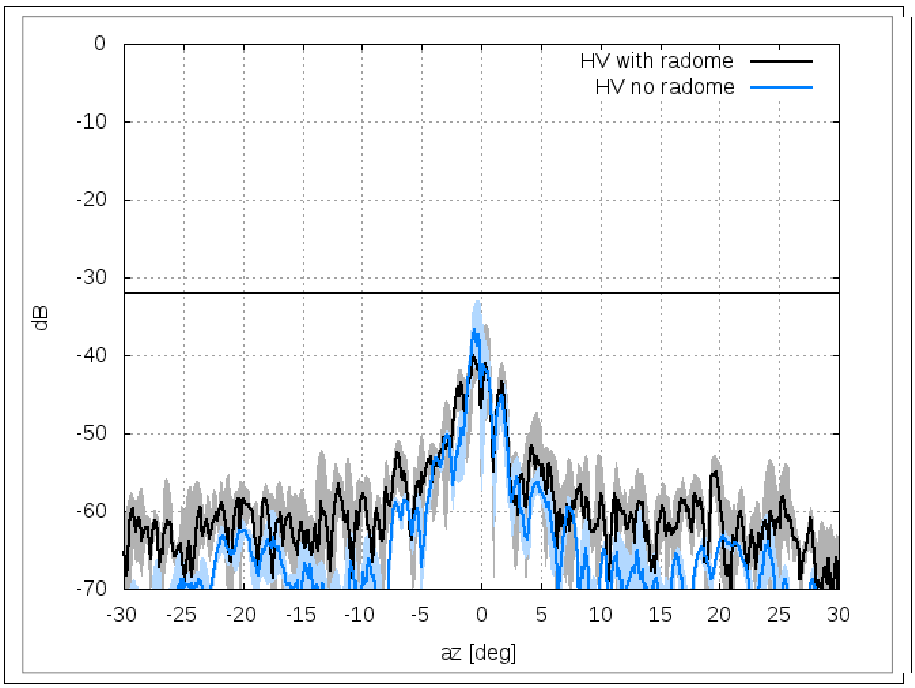

Figure 14: Variability (quartiles) of cross-polar power HV with and without radome in the main plane. Shown are also the antenna specifications.

Largest variations are usually seen near minima where slight differences in azimuthal position can cause large variations. For data without radome, side lobe peaks usually show small variations which suggest quasi-constant azimuthal locations of those peaks between

measurements. Those variations are larger for the measurements with radome. Though we have only three source sites with at three different azimuthal positions, we might argue that the increased variability seen here can be attributed to the radome. In doing so, we can relate this to an azimuthal dependence of the antenna pattern caused by the radome. This may be explained by different panel and flange combinations that are seen by the antenna aperture at given azimuthal positions. Depending on the panel combination variable scattering effects can be expected.

In the main beam area the observed variability of the cross-polar results is likely to be dominated by test range effects. Outside the main beam area we observe a similar behavior as for the copolar measurements: the variability of the cross-polar measurements is on average larger for measurements with radome. In the strut plane (denoted as +/- 45°), the antenna pattern is dominated by the presence of the struts, and the influence from the radome appears negligible (Figure 15 and 16).

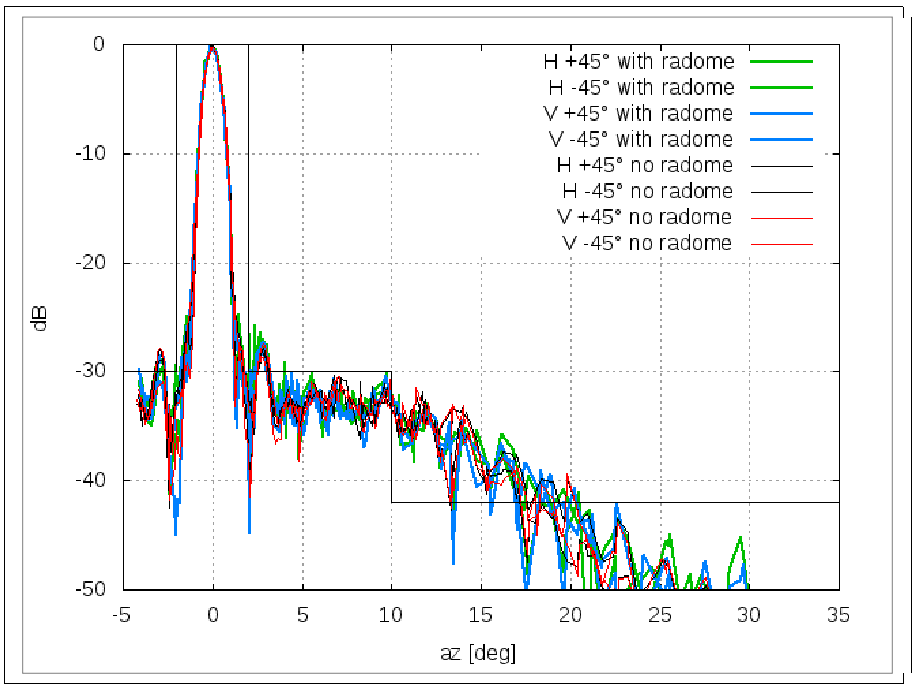

Figure 15: Average copolar power H and V in the strut plane, with and without radome. Shown are also the antenna specifications.

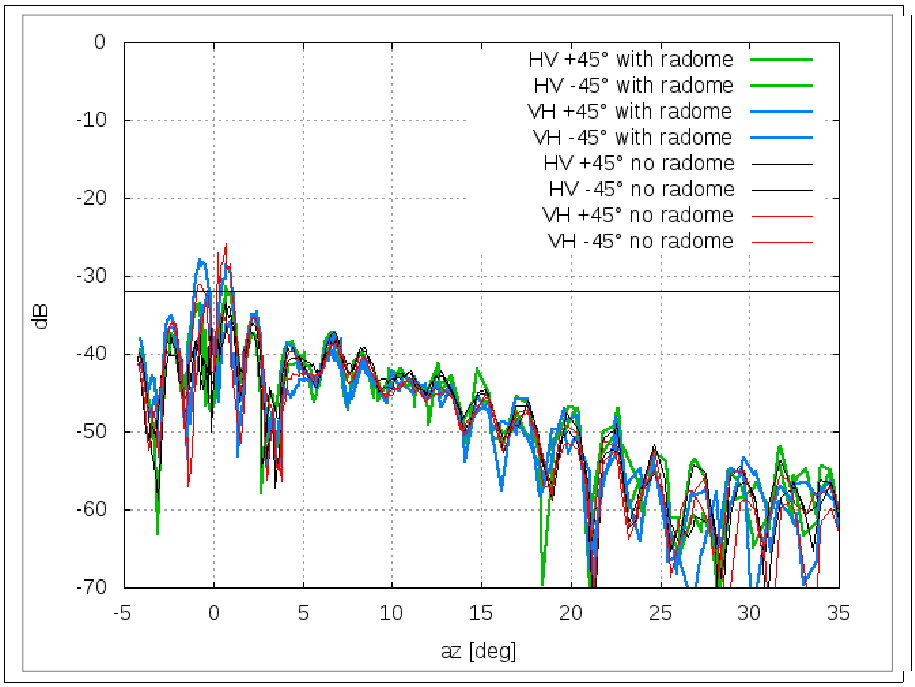

Figure 16: Average cross-polar power HV and VH in the strut plane, with and without radome. Shown are also the antenna specifications.

3.5. Measurements of differential phase and differential power

A good match of the phase and power patterns is important to obtain good quality differential phase Φdp and differential power ZDR. Especially across the main beam, where most of the energy is located, variations of differential phase and power should be small. A variability of the differential measurements would limit the accuracy of radar moments under real weather conditions. In addition, some variability can be expected due the presence of struts and errors in feed alignment (Mudukutore et al., 1995). In order to investigate the antenna performance for these aspects, SAT tests have been performed where the transmit antenna has been used in STAR mode (transmitting a linearly polarized in signal in H and V with a fixed phase difference).

In the analysis of the pattern data we compute the phase difference differential as function of radial distance in the main beam. The center or zero radial distance is defined as the location of the SNRh peak power. For a given radial distance interval we compute the statistics of the data from all angles. This is done individually for all data with and without radome. The results based on the three source sites are then averaged to obtain the overall distribution of the phase difference in the main beam area. For the differential phase the results are shown in Figure 17.

Up to about a radial distance of 1°, variations of differential phase are small for the measurements without radome. At about 1° we find a mean difference of -2° relative to the peak value in the main beam center. This corresponds to SNR values of about -15 dB below the main peak. Differences start to increase from about r = 0.7° on, which also coincides with increased variability as seen in the 1st and 3rd quartile values. Up to this value the phase difference is quasi-constant over the main beam. The measurements with radome on average show a somewhat larger increase in phase difference in the main beam area. Also the 1st and 3rd quartiles indicate a larger range suggesting an increased variability in differential phase due to the radome.

The largest variability in differential phase is found around r ~ 1.8° where we find the first minium in received copolar power (below -30 dB in SNRh).

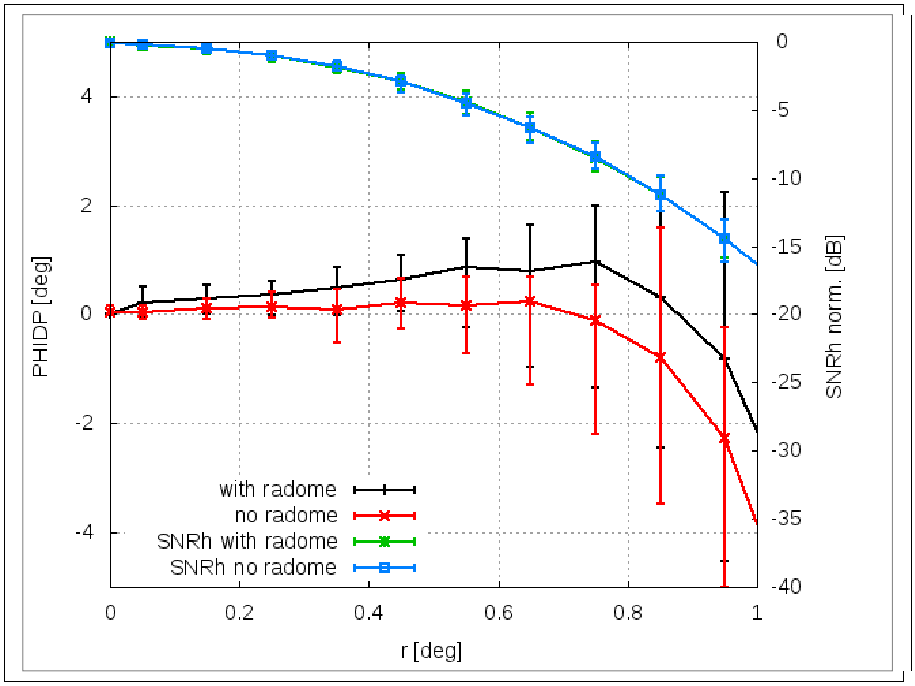

Figure 17: The differential phase without and with the radome as a function of radial distance relativeto the main SNR peak. Shown are the median and the 1st and 3rd quartiles, respectively based on the pattern data from the three source sites. The upper panel shows the full range, whereas the lower panel shows a narrowed range in phase in order to see the differences in the main beam area.

The results for differential power are shown in Figure 18. On average, differential power is essentially 0 dB up to a radial distance of r = 0.5°, which roughly corresponds to the 3dB beam width. This is found for the measurements with and without radome. With increasing radial distance r, the power difference increases up to ~ 0.7 dB at r = 1°. The increase is larger with radome where we reach a power difference of about ~ 1 dB at r = 1°. If the

scattering volume is not beam-filling or heterogeneous, the observed differential power variability may affect the resulting data quality of ZDR (likely more than for the differential phase measurements).

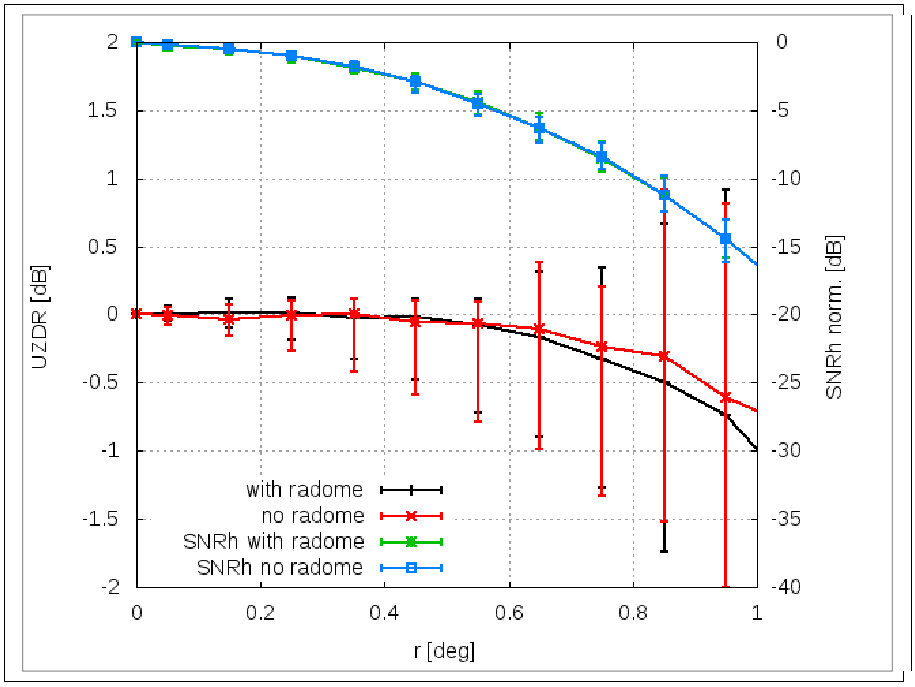

Figure 18: The differential power without and with the radome as a function of radial distance relativeto the main SNR peak. Shown are the median and the 1st and 3rd quartiles, respectively based on the pattern data from the three source sites. The upper panel shows the full range, whereas the lower panel shows a narrowed range in differential power in order to see the differences in the main beam area.

3.6. Beam squint and beam width

Beam width and beam squint are important characteristics of an antenna. We compute the beam width from the 3-D data by extracting the location of the -3 dB isoline relative to the peak of the main beam. All the computed beam widths are all below 1°. The results show that the beam widths in V are on average somewhat larger than th beam widths in H: without radome 0.90° (H) versus 0.93° (V), with radome 0.88° (H) versus 0.91° (V).

In order to compute the beam squint, we initially determine the position of the V peak relative to the main peak position in H. Then we fit a 2-D surface to the SNR data from which the peak positions in H and V are calculated. Those data are used to compute the beam squint. The uncertainty of the beam squint is determined by the uncertainties of the surface fit. It should be noted that we the results actually represent the one-way beam squint. The beam squint with radome is always smaller than 0.04°, whereas two measurements without radome show a somewhat larger squint, but still below the specified 0.06°.

3.7. Summary

We find that the beam width, shape and squint do not degrade due to the radome. This in turn also means that the gain of the antenna should not deteriorate. The first side lobe level is raised in one polarization plane compared to measurements without radome. The side lobe levels are raised significantly by the radome off the main beam, but the resulting levels are on average still within the specifications. The STAR mode tests indicate that the inhomogeneity of differential phase in the main beam is larger due to the radome. The larger inhomogeneity appears related to different panel combinations seen by the antenna aperture considering the three source sites. This in turn implies some azimuthal variability of the radar moments which still has to be quantified. The differential power measurements indicate a very good match up to the -3 dB level of the main beam. The power difference for the measurements with radome becomes larger with increasing radial distance (up to 1 dB). Here we may be left with a larger ZDR bias due to the radome especially for situations with non-beam filling targets. The large variability of the cross-polar data between the source sites at low elevations also implies that the achievable LDR in a stratiform rain situation may be quite variable depending on the propagation of the transmitted and received signals of the radar system.

4. Processing algorithms

The raw polarimetric variables are affected by a number of errors that must be corrected. They can be expressed as:

$$Z_h^{obs}(r) = Z_h(r) + \Delta_{Z_h} + \sigma_{Z_h} - 2\int_0^r A_h(r)\,dr - 2A^{radome}$$

$$Z_{dr}^{obs}(r) = Z_{dr}(r) + \Delta_{Z_{dr}} + \sigma_{Z_{dr}} - 2\int_0^r A_{dp}(r)\,dr - 2A_{dp}^{radome}$$

$$\Psi_{dp}^{obs}(r) = \phi_{dp}(r) + \delta_{co}(r) + \phi_{dp_o} + \sigma_{\phi_{dp}}$$

$$\phi_{dp}(r) = 2\int_0^r K_{dp}(r)\,dr$$

$$\rho_{hv}^{obs}(r) = \rho_{hv}(r) + \sigma_{\rho_{hv}}$$

In these equations σ_x represents the standard deviation of the observation caused by the system fluctuation errors, residual ground clutter, etc., Δ_x represents the uncertainties in the calibration of the various channels, including the cross-coupling error due to the simultaneous transmission and reception of the vertically and horizontally polarized signals (Hubbert et al.,

2010), A_h is the specific attenuation, A_{dp} is the specific differential attenuation. The superscript *radome* stands for the attenuation caused by the radome, δ_{co} is the backscattering copolar differential phase, and Φ_{dpo} is the system differential phase offset. In addition to these sources of uncertainty one should not forget orographic effects like partial beam blocking, etc. The polarimetric pre-processing chain attempts to correct for the contributions of the different sources of uncertainty and provide the best estimation of Z_h, Z_{dr}, ρ_{hv} and K_{dp}, which contain the microphysical information required to perform attenuation correction, identify the echo type, and quantify the precipitation rate.

4.1. Polarimetric variables processing at Météo France

The inputs of the polarimetric pre-processing chain are the raw polarimetric variables computed from digitised I and Q data by an in-house developed radar processor, Castor2 (Parent-du-Châtelet et al. 2001). The processor provides horizontal reflectivity Z_h, differential reflectivity Z_{dr}, co-polar correlation coefficient ρ_{hv} and differential phase Φ_{dp} in polar coordinates (resolution 240m x 0.5°), as well as the pulse-to-pulse reflectivity fluctuation σ_z (Sugier et al. 2002) in Cartesian coordinates (resolution 1 km^2).

The polarimetric chain processes each PPI separately except for the bright band identification, which is based on the examination of several consecutive volume scans. The raw polarimetric data undergoes the following processing steps in sequential order:

- **Azimuth-dependent Z_{dr} bias correction** based on a-priori calculated curves (see Section 2.2).
- **Signal-to-Noise Ratio (SNR) estimation and correction of Z_{dr} and ρ_{hv} for low SNR biases** (Gourley et al. 2006).
- **Pre-classification of each polar pixel in either Clear Air (CA), Ground clutter (GC) or Precipitation (PR)** according to the results of a fuzzy logic algorithm using the Z_{dr} texture, σ_z and ρ_{hv} as described in Gourley et al. (2007a).
- **Calculation and correction of the system differential phase Φ_{dpo}**. Φ_{dpo} is calculated dynamically for each ray.
- **De-speckling of PR pixels**. The spatial homogeneity of the precipitation is considered on a gate by gate basis in order to potentially re-classify misclassified echoes.
- **Bright band identification** following the method described in Tabary et al. (2006), which is based on a combination of ρ_{hv} and model-produced freezing level height.

A temporal filter propagates the information from scan to scan and time to time. If the identification is successful, this algorithm provides the bright band base altitude and the bright band thickness, otherwise default altitude and thickness are used.

- **Filtering of Φ_{dp} in precipitation with a moving median filter**. A median filter is applied to the ±12 consecutive range gates surrounding a gate classified as PR. This corresponds to a filtering length of 6 km. If there are less than 13 gates (i.e. 50% of the total number of gates in the window) classified as PR the median is not calculated. In that case, the filtered Φ_{dp} value is obtained as a linear interpolation of the surrounding valid filtered gates.
- **Calculation of K_{dp} based on a 25 PR range gates linear regression over the filtered Φ_{dp} curve.**
- **Precipitation-induced attenuation correction**. Both A_h and A_{dp} are considered linearly proportional to Φ_{dp}. The coefficients at C band were determined empirically using data from the Trappes Radar (see Gourley et al. 2007b). The values that have been found are: γ_{dp}=0.03 dB/° and γ_h=0.08 dB/°. For S-band, coefficients provided in Bringi and Chandrasekar (2001) are: γ_{dp}=0.04 dB/° and γ_h=0.004 dB/°. The coefficients at X-band radar were extracted from joint S-band/X-band measurements (see Tabary et al. 2008): γ_{dp}=0.04 dB/° and γ_h=0.28 dB/°.
- **Precipitation classification using a fuzzy logic scheme**. Precipitating echoes are currently divided in weak, moderate and strong rain, dry and wet snow, ice, graupel, hail, rain-hail mixture and big drops.

The polarimetric chain therefore provides the following output variables: Z_{dr} and Z_h corrected for attenuation, Z_{dr} and Z_h not corrected for attenuation, the Path Integrated Attenuation (PIA) and the Path Integrated Differential Attenuation (PIDA), ρ_{hv}, K_{dp}, filtered and non-filtered offset corrected $\Phi_{dp,}$ σ_z, Z_{dr} texture, and echo type classification. All these variables are in polar coordinates with a resolution of 240 m x 0.5°. In addition the echo type classification, the PIA and the Z_h corrected for attenuation are also expressed in 1 km^2 Cartesian coordinates.

5. Quantitative Precipitation Estimation

5.1. Overview of existing polarimetric QPE algorithms

Polarimetric QPE algorithms are either based on Z_h, on Z_{dr}, on K_{dp} or on a combination of two or three of those parameters. The first family of algorithms are the Z_h-R relationships ($Z=aR^b$). In that case, the benefit brought by polarimetry is the correction for attenuation using Φ_{dp} (Gourley et al. 2007b), which leads to better results than iterative approaches using A_h-Z_h relationship (Hitschfeld and Bordan 1954). The parameters *a* and *b* are typically determined empirically using long series of disdrometer data. The most widely used Z_h-R relationships are the Marshall-Palmer (1948) (*a*=200, *b*=1.6) and the one used by the WSR-88D radars (a=300, b=1.4) (Fulton et al. 1998). The Marshall-Palmer Z-R relationship is the base of the current Météo France radar rainfall rate product.

A second class of estimators consists in relationships of the type $R=a_1 Z_h^{b1} Z_{dr}^{c1}$ where a_1, b_1 and c_1 are three constants (see Gorgucci et al. (1994) for example). The performance of that class of algorithms is dependent upon the ability to provide Z_{dr} estimates with minimal standard deviation and bias. Tabary et al. (2011) show that a 0.2 dB bias in Z_{dr} results in a 15% increase on the retrieved rainfall rate bias. In order to minimize the impact of noise on Z_{dr} estimates, some spatial averaging / integration can be performed. This is what is done by the so-called Z-Z_{dr} algorithm proposed by Illingworth and Thompson (2005). This algorithm attempts to adapt the *a* factor in the Z-R relationship to the actual drop size distribution, which is proportional to the square root of N_w, the normalized drop concentration. The factor *b* is considered constant with a value of 1.5. The algorithm derives the N_w of an area by obtaining the areal Z_{dr} that best fits into one of the a-priori Z_h-Z_{dr} curves calculated from a particular N_w. The scatter of the points around the best fit provides the error in the derived value of *a* and, subsequently, in the retrieved rainfall rate.

The use of K_{dp} retrieval algorithms of the type $R=f(K_{dp})$ has been widely reported in literature (see for example Sachidananda and Zrnic, 1987). Below a wavelength-dependent threshold on the precipitation rate (typically 2 mm h^{-1} at X-band, 5 mm h^{-1} at C-band and 10 mm h^{-1} at S-band), the range variation of Φ_{dp} becomes comparable with the measurement phase noise (a few degrees for operational scanning radars) and the K_{dp} estimations become of poor quality. Consequently, $R=f(K_{dp})$ algorithms are usually used in combination with Z-R relationships. Note that $R=f(K_{dp})$ algorithms are immune to radar calibration errors, partial beam blocking, attenuation by precipitation or wet radome, … That feature makes this class

of algorithms particularly attractive at wavelengths such as C or X band. Moreover, the K_{dp}-based estimator is less sensitive than the Z_h-based to changes in the DSD since it depends on its 4^{th} moment (vs. 6^{th} for Z_h, Ryzhkov and Zrnic 1996).

The ZPHI algorithm aims at correcting radar data for attenuation and taking into account DSD fluctuations in rainfall estimation. It has been described in detail by Testud et al. (2000) and its superiority over conventional (ZR) rain rate estimation techniques has been objectively demonstrated using rain gauges (Le Bouar et al. 2001).

Finally, attempts have been made to combine all the polarimetric variables together in order to exploit at most the polarimetric information. Rhyzkov et al. (2005) used a combination of the different algorithms and Vulpiani et al. (2009) used a neural network to retrieve the DSD parameters from polarimetric data. Hogan (2007) developed a variational scheme which uses a forward model of Z_{dr} and Φ_{dp} and iteratively retrieves the coefficient *a* in the Z-R relationship by minimizing the root mean square (RMS) error between the measured and the forward-modelled polarimetric variables. This algorithm also corrects for attenuation by including its effects in the forward model and provides an estimation of the rainfall rate error.

5.2. Algorithm evaluation methodology at Météo France

A modular method has been developed to evaluate the QPE algorithms. The first step is the estimation of the instantaneous rainfall rate in regions that have been classified as rain, dry or wet hail and big drops using one of the various algorithms implemented. The other regions of the radar domain are assigned a No Data Available (NA) value. The reason for allowing the presence of hail is that several studies (e.g. Tabary et al. 2010) have shown that discrimination between hail and heavy rain at C-band is not trivial, and robust algorithms are still under development. It should be noted though, that hail is a rare phenomenon, so including that hydrometeor type in the analysis should not bias the results too much. The outputs of the algorithm are then transformed from polar to Cartesian coordinates using a Cressman interpolation scheme. The Cressman radius is set to 660 m up to 50 km and then increases linearly with range. The pixels that were classified as noise or clear air by the polarimetric chain are then re-classified as valid pixels with a rain rate of 0 mm h^{-1}.

By analysing the displacement of the precipitation cells from one scan to the next one (5' later), 2D advection fields can be determined and used to over-sample the data (Tuttle and Foote 1990 and Tabary 2007). The 2D advection field is subsequently used to advect the 5' radar rainfall rate maps by 30 s increment steps. 10 new images are thus created (one every 30

s) from the original image and added to each other to yield the 5’ rainfall accumulation. Finally the hourly rainfall accumulation is obtained by adding the twelve 5’ rainfall accumulation images. If one 5’ accumulation pixel is classified NA within the hour, then the hourly accumulation for that pixel is considered to be missing. That very strict criterion was introduced in order not to bias the evaluation results.

In order to ease the interpretation of results, only one elevation angle is used to generate the radar QPE maps, which thus differ from what is operationally produced (Tabary 2007). The selection of the elevation angle is a compromise between minimizing beam height over the ground and minimizing partial beam blocking and ground clutter effects. The percentage of beam blockage is simulated using a digital terrain map (Delrieu et al. 1995). As an additional criterion, when necessary, regions with beam blocking exceeding 10% are excluded from the comparison. The evaluation is carried out hourly on a day-by-day basis. For practical reasons, the last hour of each day (from 23:00 to midnight UTC) is not considered.

The hourly rainfall accumulation Cartesian maps obtained by the QPE algorithms are compared against hourly rain gauges. The Météo France rain gauge network consists of tipping bucket gauges with a bucket resolution of 0.2 mm, i.e. the minimum hourly rainfall accumulation that can be measured is 0.2 mm. All rain gauge data are routinely quality-controlled. An automatic control analyses the coherence respect to the 6’ measurement and the daily measurement. The spatial coherence of the daily measurement is also analysed, and an expert corrects the values of the hourly measurement when required. Additional expert analysis take place regularly. Nevertheless, rain gauges, like any other measurement instrument, suffer from uncertainties. Ciach (2003) attempted to quantify the measurement error committed by tipping bucket rain gauges of the type used by Météo France. Ciach (2003) found that the relative error of the measurement was inversely proportional to the rainfall rate and could be modelled as:

$$\sigma_m(\Delta T, G) = e_o(\Delta T) + \frac{R_o(\Delta T)}{G}$$

with e_o and R_o being model coefficients depending on the time scale ΔT of the measurement. For the hourly accumulation e_o and R_o were found to be 0.002 and 0.19 mm respectively.

The radar-rain gauge comparison is done by matching each rain gauge with the corresponding radar pixel. The fact that the radar retrieval is an areal measurement whereas the rain gauge is a point measurement introduces an extra degree of uncertainty. Emmanuel et al. (2011) attempted to model such representativeness error. They assumed that it is

proportional to the variance of the rainfall field with the constant of proportionality dependent on ΔT. For the one hour accumulation they found:

$$\sigma_s = 0.14\sigma_{rain}$$

The main issue of the methodology is to estimate the variance of the rain field. The approach by Emmanuel et al. (2011), and the one we followed here, was to consider the variance between the rain gauges in the area as the actual variance of the rain field. Admittedly there are questions about the representability of such methods since what is of interest is the variance of the rain field at the pixel scale (1 km^2), whereas what is actually calculated is the rainfall field variance of the area under study and the reliability of such estimation depends on the density of the rain gauge network at disposal. Nevertheless, such methodology still provides a qualitative measurement of the representativeness error. The combination of the measurement error of the rain gauges and the representativeness error provides the confidence interval of the rain gauge measurements estimated later on in this paper.

In order to minimize possible Vertical Profile of Reflectivity (VPR) effects, which are uncompensated, the comparison is restricted to ranges below 60 km from the radar. There are typically between 30 and 50 rain gauges in the comparison area.

The quality of the algorithms is evaluated using the normalized bias (NB) between the rain gauge and the radar rainfall accumulation defined as:

$$NB = \frac{\langle R \rangle}{\langle G \rangle} - 1$$

where <> denotes the average, the correlation (corr):

$$corr = \frac{\sum_{\forall i} \left(G_i - \langle G \rangle\right)\left(R_i - \langle R \rangle\right)}{\sqrt{\sum_{\forall i} \left(G_i - \langle G \rangle\right)^2} \sqrt{\sum_{\forall i} \left(R_i - \langle R \rangle\right)^2}}$$

the root mean square error (RMS):

$$RMS = \sqrt{\frac{\sum_{\forall i} \left(R_i - G_i\right)^2}{n}}$$

and the Nash-Sutcliffe model efficiency coefficient (Nash):

$$Nash = 1 - \frac{\sum_{\forall i} \left(R_i - G_i\right)^2}{\sum_{\forall i} \left(G_i - \langle G \rangle\right)^2}$$

In addition, the percentage of radar measurements included within the confidence interval of the rain gauge measurements, i.e.

$$\%R_i \in [G_i - \sigma_{toti}, G_i + \sigma_{toti}]$$

where

$$\sigma_{toti}^2 = \sigma_{si}^2 + \sigma_{mi}^2$$

has also been calculated.

5.3. Results of evaluation of two integrated methods

Dataset

The algorithms have been implemented on the French C-band polarimetric Trappes radar, located in the region Ile de France. The region around the Trappes radar is densely equipped with several rain gauge networks managed by several authorities, including Météo France and water sewage agencies. Overall, there are about a hundred rain gauges recording hourly rainfall accumulation within a distance of 100 km from the radar site.

Table 1 Overview of the 12 episodes used in the evaluation

Date (DD/MM/YYYY)	Time (UTC)	0°C isotherm height [m above sea level]	maximum hourly rain gauge accumulation [mm]	Type of the rainfall
06/04/2005	13.00-24.00	1900	10,8	mixed
18/04/2005	00.00-23.00	1900	3,2	stratiform
24/04/2005	00.00-14.00	2100	16	mixed
26/04/2005	13.00-24.00	2000	8,2	stratiform
14/05/2005	00.00-23.00	2400	10,4	mixed
23/06/2005	07.00-23.00	3900	38,6	convective
26/06/2005	00.00-23.00	4200	50,7	convective
28/06/2005	15.00-23.00	4000	23,6	convective
30/06/2005	10.00-23.00	2900	23,6	convective
04/07/2005	00.00-24.00	2900	16	mixed
28/07/2005	14.00-23.00	3900	32,2	convective

The experimental period took place during the year 2005. The 11 most intense and interesting events of this year were selected for the evaluation of the two algorithms (Table 1).

Notice however, that they are not all convective nor concentrated to the summer. For the comparison to be meaningful and significant, it is important to embrace a wide variety of precipitating systems. During the second part of June, several storms affected the Paris region. The most spectacular event of deep convection happened on the 23 June 2005 with a maximum hourly rainfall measured at a rain gauge of 51 mm. A second event, the 26 of June, generated a maximum hourly rainfall of 38.6 mm at a rain gauge location. The hundred-year and ten-year return period of hourly rainfall in the region Ile-de-France are about 55 mm and 37 mm respectively. Thus, the validation data set contains two very intense events, typical of rain storms causing flash-floods on small to medium size urbanised catchments of this region.

Evaluated algorithms

Attenuation-corrected conventional estimator (CONV_ATT_BY_PDP): This estimator is exactly the same the conventional estimator described before except that it uses attenuation-corrected horizontal reflectivities (Z_H).

Rain gauge adjusted conventional estimator (CONV_RG_ADJUSTED): This estimator is a rain gauge adjusted version of the conventional estimator (CONV). The gauge adjustment scheme that is used is the strict reproduction of what is done operationally at Météo France (Tabary, 2007) evaluated in the Paris region by Emmanuel et al. (2011), which makes this estimator a critical benchmark to beat in the present study. The adjustment scheme consists in applying one single calibration factor (CF) to the entire 5' radar 1 km² Cartesian QPE map. The calibration factor that is applied to all incoming 5-minute radar QPE of hour k+1 is updated at the end of hour k (upon reception of rain gauge accumulations for the hour k) as follows:

$$CF_k = \frac{\sum_{i=k-M}^{i=k} \omega_i \left(\sum_{j=1}^{j=n_i} P_{i,j}\right) + CONSTANT}{\sum_{i=k-M}^{i=k} \omega_i \left(\sum_{j=1}^{j=n_i} R_{i,j}\right) + CONSTANT}$$

where $P_{i,j}$ are the j=1 … n_i available hourly rain gauge accumulations with good visibility from the radar (i.e. typically located within 80 km from the radar) for the hour i and $R_{i,j}$ are the co-located radar raw accumulations for the same hour (i). M represents the memory of the algorithm that is to say the number of hours before the hour k which are taken into account in the computation. $\omega_i = 2^{(-(k-i)/4)}$ represents the weight given to radar and rain gauge accumulations of hour i. M is set to 40 (hours). Consequently, hourly accumulations of hour k (resp. k-4, k-16 and k-40) receive a weight of 1 (resp. 0.5, 0.0625 and 0.0009765625). The

term named CONSTANT in the equation is the term that forces the calibration factor to go back to unity after each episode. It also avoids unrealistic short-term "yo-yo like" variations of the calibration factor in case of low rain rates and / or small-scale rain systems poorly sampled by the rain gauge network. CONSTANT is set in the algorithm to 10 mm.

Rain gauge adjusted attenuation-corrected conventional estimator (CONV_ ATT_BY_PDP _RG_ADJUSTED): This estimator is the attenuation-corrected conventional estimator (CONV_ATT_BY_PDP) to which the rain gauge adjustment scheme describes above is applied.

ZZDR with attenuation correction (ZZDR_ATT_BY_PDP)

ZPHI (ZPHI)

Evaluation results

Figures 19 and 20 illustrate quite well the performances, advantages and drawbacks of the various estimators on two contrasted cases: a pure stratiform case with low to moderate rain rates (18th of April, Fig. 19) and a mixed convective / stratiform Summer case with rain rates exceeding 10 mm h^{-1} (4th of July, Fig. 20). Each plot corresponds to one of the 6 tested algorithms and provides, in addition to the entire set of [radar, rain gauge] couple values, the "all rain rates" NB (first line), the NB for rain rates above 1 mm h^{-1} (second line), the "all rain rates" correlation (third line), the correlation for rain rates above 1 mm h^{-1} (fourth line). The number of [radar, rain gauge] couples is also indicated on each plot. Notice that the horizontal and vertical scales are logarithmic.

In the former case (Fig. 19), the conventional estimator (CONV) appears to be severely negatively biased ("all rain rates" NB is equal to -0.4, i.e. -40%). The attenuation correction (CONV_ATT_BY_PDP) does not change anything to that negative bias given that there is no attenuation on that case). The gauge adjustment scheme helps reducing a small fraction of that bias (the "all rain rates" NB of CONV_RG_ADJUSTED is equal to -0.25, i.e. -25%). The reason why the bias is not fully removed by the gauge adjustment scheme is because the hourly rainfall accumulations are not high enough to "trigger" the gauge adjustment scheme and the calibration factor (CF) essentially remains equal to unity all over thee episode. On that case, the ZZDR algorithm (ZZDR_ATT_BY_PDP) performs remarkably well and the "all rain rates" NB is equal to 0 while the correlation remains quite high (0.80), yet slightly below the correlation obtained with the conventional estimator (0.82). On the basis of that example, one can illustrate the potential of polarimetry for radar hydrology, namely its ability to adjust in real-time for the Z-R relationship variability and provide unbiased QPEs, which is a

mandatory requirement for subsequent use in any hydrologic forecasting system. One requirement for that is that the radar variables (Z_H and Z_{DR}) have to be well calibrated. On that stratiform case with low to moderate rain rates (hence with almost no differential phase shift), ZPHI is hardly triggered and the negative NB hardly removed (ZPHI "all rain rates" NB is equal to -0.36, i.e. -36%).

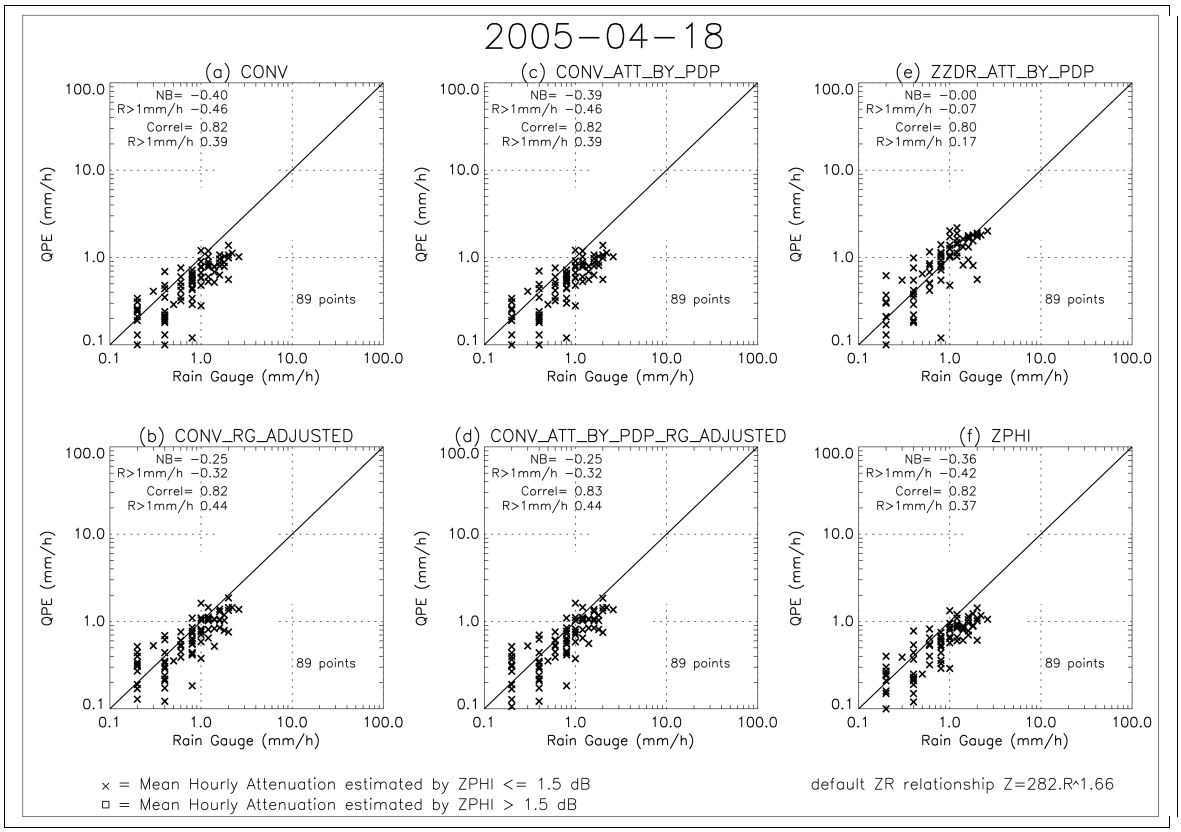

Figure 19 Results obtained for the 18th of April case (stratiform) with the 6 algorithms.

The second case (4th of July, Fig. 20) reveals again a strong underestimation of the conventional estimator (CONV), which has an "all rain rates" NB of -0.42 (-42%). The gauge adjustment is this time much more efficient and allows significantly reducing this negative bias ("all rain rates" NB of CONV_RG_ADJUSTED becomes equal to -0.13). At the same time, the attenuation correction also contributes to reducing the bias, yet in a lower proportion ("all rain rates" NB of CONV_ATT_BY_PDP is still equal to -0.35). The attenuation correction improves the correlation, especially for rain rates above 1 mmh^{-1}. ZZDR removes about half of the negative bias obtained with the conventional estimator ("all rain rates" NB of ZZDR_ATT_BY_PDP is -0.21). ZPHI appears to be clearly the best estimator on that case with a bias that is close to zero and a correlation that is increased with respect to all other estimators. The very good performance of ZPHI on that case is clearly related to the fact that

the rather high (according to the Paris region standards) rain rates observed are leading to significant differential phase shifts and, subsequently, frequent triggering of the algorithm.

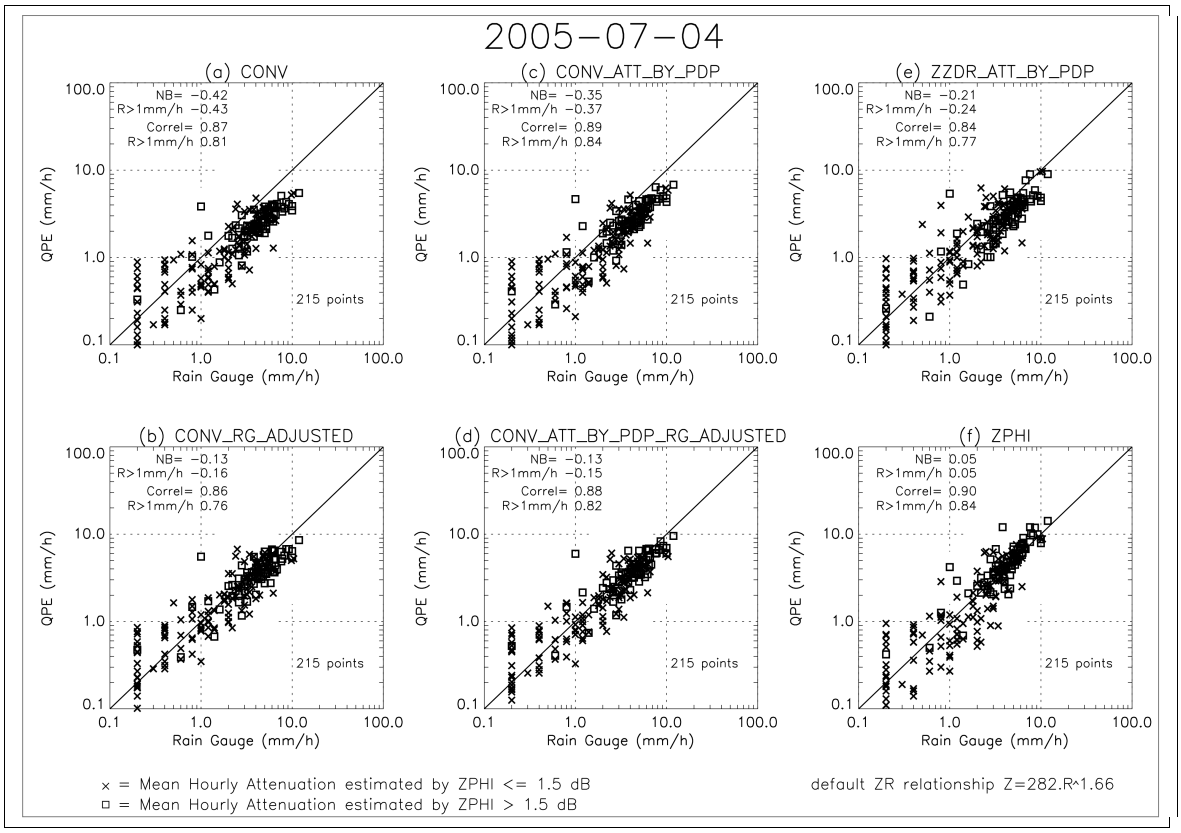

Figure 20 Results obtained for the 4th of July case (convective – stratiform) with the 6 algorithms

The global results obtained on all 11 episodes are presented on Fig. 21. The layout of Fig. 21 is exactly the same as Figs. 19 and 20, except that, in addition to the NB and the correlation coefficient, values of the Root Mean Square Error (RMS) are also provided for each plot (second column) for “all rain rates” (first line) and for rain rates above 1 mm h^{-1} (second line). The conventional estimator (CONV) is negatively biased (“all rain rates” NB is equal to -0.34). Overall, the gauge adjustment performs well (CONV_RG_ADJUSTED) and allows reducing that negative bias down to -0.09 (“all rain rates” NB). The attenuation correction (CONV_ATT_BY_PDP) improves the correlation with respect to the conventional (CONV) estimator (“all rain rates” correlation goes from 0.82 to 0.84), while slightly removing the negative bias (NB going up from -0.34 to -0.24). Finally, the attenuation-corrected and gauge adjusted conventional estimator (CONV_ATT_BY_PDP_RG_ADJUSTED) and the two polarimetric estimators (ZZDR_ATT_BY_PDP and ZPHI) obtain exactly the same “all rain rates” correlation (0.8) and a close-to-zero “all rain rates” NB (-0.08 for CONV_ATT_BY_PDP_RG_ADJUSTED and ZPHI and 0 exactly for ZZDR_ATT_BY_PDP). The “all rain rates” RMS errors are

ranked as follows (from highest to lowest): 2.02 mm (CONV, Fig. 21a), 1.86 mm (CONV_RG_ADJUSTED, Fig. 21b), 1.75 mm (CONV_ATT_BY_PDP, Fig. 21c), 1.71 mm (ZZDR_ATT_BY_PDP, Fig. 21e) and finally 1.65 mm (CONV_ATT_BY_PDP_RG_ADJUSTED and ZPHI, Figs. 71d and 21f). In terms of RMS error, ZZDR is thus slightly below ZPHI and CONV_ATT_BY_PDP_RG_ADJUSTED.

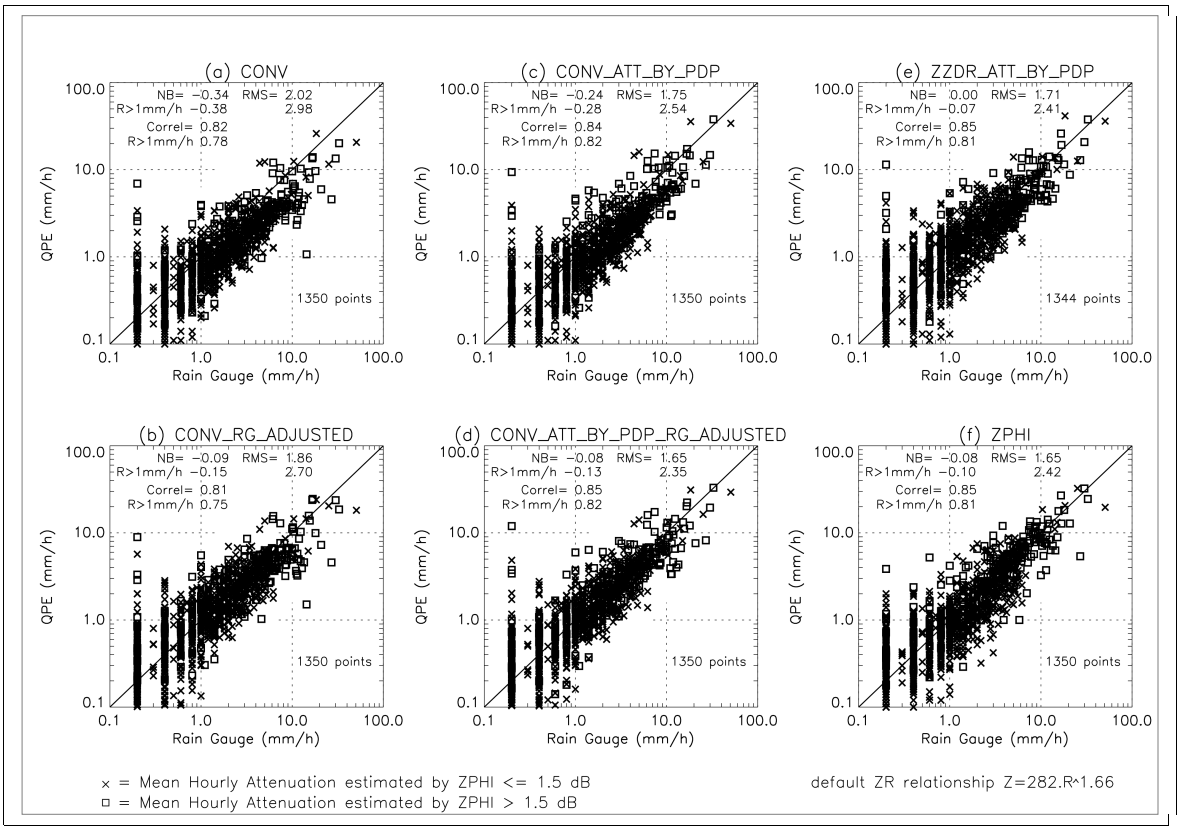

Figure 21 Global results obtained over the 12 events of 2005 with the 6 algorithms

Two further statistics have been produced in order to assess the specific behavior of the various estimators under different rain rate regimes and different measurement conditions: Fig. 22 shows for each estimator the median value of the NB for different classes of hourly rain gauge accumulations (< 1 mm, 1 – 5 mm, 5 – 10 mm, > 10 mm). All the intense rain rates measured during the convective events which occurred in June and July 2005 are grouped in the class >10 mm. Figure 23 shows, also for each of the 6 estimators, the median radar – rain gauge ratio (1+NB) for different mean hourly attenuation (< 1.5 dB, 1.5 – 3 dB, > 3 dB).

The stratification with rain gauge accumulations (Fig. 22) confirms the overall tendency to underestimate of the conventional estimator (CONV), which tends also to become more negative for high rainfall rates (median radar – rain gauge ratio equal to 0.46 for hourly rain gauge accumulations larger than 10 mm h^{-1}). The correction for attenuation (CONV_ATT_BY_PDP) tends to make the median radar – rain gauge ratio curve flatter

across the hourly rain gauge accumulations range. The remaining negative slope of the radar – rain gauge ratio as a function of hourly rain gauge accumulations is probably to be attributed to the fact that the exponent of the default Z-R relationship ($Z=282R^{1.66}$) is not appropriate for the Spring and Summer cases considered in this validation exercise. A lower exponent, say 1.4 or 1.5, would lead to a median radar – rain gauge ratio stable across the whole range of hourly rain gauge accumulations. The gauge adjustment has a positive impact when applied to either conventional estimator (CONV_RG_ADJUSTED) or to the attenuation-corrected conventional estimator (CONV_ATT_BY_PDP_RG_ADJUSTED). A fraction of the underestimation is removed. However, the gauge adjustment scheme is unable to make the radar – rain gauge ratio stable across the range all hourly rain gauge accumulations and a negative slope of the median radar – rain gauge ratio versus the hourly rain gauge accumulation remains. The two polarimetric estimators appear to be complementary, with ZZDR_ATT_BY_PDP performing better than ZPHI (and as good as the two gauge-adjusted estimators) for low to moderate hourly rain gauge accumulations (up to 5 mm h^{-1}) and ZPHI over-performing all other estimators for hourly rain gauge accumulations exceeding 5 mm h^{-1}.

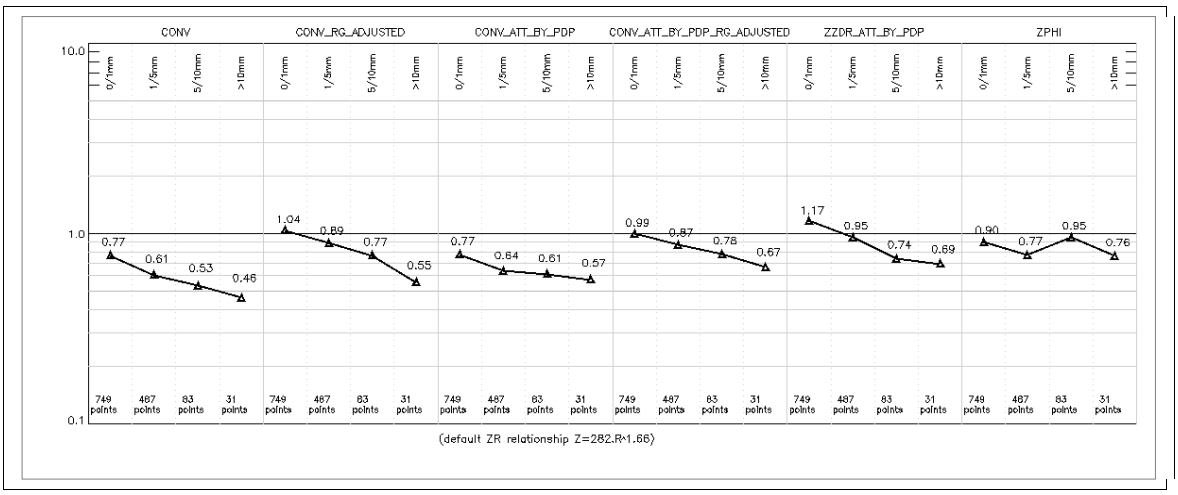

Figure 22 median normalized bias radar – rain gauge ratio (1+NB) stratified according to the various estimators and to the hourly rain gauge accumulation. The vertical scale is logarithmic.

The stratification with mean hourly attenuation (Fig. 23) evidences a clear underestimation building up with the conventional estimator (CONV) as the mean hourly attenuation increases. When attenuation is corrected for (CONV_ATT_BY_PDP), the median radar – rain gauge ratio becomes almost independent from the mean hourly attenuation, which demonstrates the performance of the attenuation correction scheme. The gauge adjustment

scheme reduces the underestimation but not the tendency for the median radar – rain gauge ratio to depart (negatively) from unity with increasing mean hourly attenuation. Finally, on that statistics, ZZDR_ATT_BY_PDP over-performs all other estimators up to a mean hourly attenuation of 1.5 dB Between 1.5 and 3.0 dB, ZZDR_ATT_BY_PDP and ZPHI are equivalent and beyond the 3 dB threshold, as expected, ZPHI becomes the best estimator.

As a conclusion, the results obtained with the two polarimetric estimators (ZZDR_ATT_BY_PDP and ZPHI), which do not include at all any rain gauge adjustment and are based solely on radar data, are very positive. Both estimators perform as well, if not clearly better, than the gauge-adjusted conventional estimator. ZZDR_ATT_BY_PDP appears to be the best estimator for low to moderate hourly rain gauge accumulations (up to 5 mm h^{-1}) and ZPHI is the best one beyond. Those conclusions rely however on the very strong assumption that the polarimetric variables, Z_H and Z_{DR}, are well calibrated.

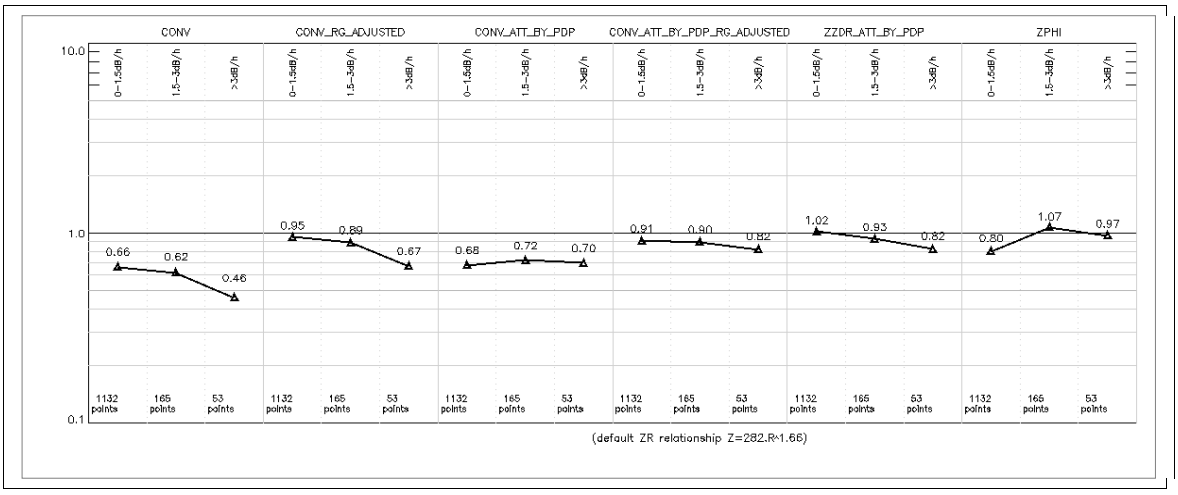

Figure 23 median normalized radar – rain gauge ratio (1+NB) stratified according to the various estimators and to the mean hourly attenuation. The vertical scale is logarithmic

To assess the sensitivity of ZZDR_ATT_BY_PDP with respect to biases on Z_{DR}, the accuracy of which is quite a challenge to guarantee with operational polarimetric radars, two experiments were conducted in which 1) a positive (resp. negative) bias of 0.2 dB (resp -0.2 dB) was added to all Z_{DR} data (previously corrected for the azimuth-dependent biases) the ZZDR_ATT_BY_PDP was applied to the new datasets. The results, in terms of NB and CORR, are presented in Tab. 2. Except on a few cases (23 June 2005, 28 July 2005), the correlation does not change with the bias. The NB on the other hand is extremely reactive: typically a bias of +0.2 dB (Z_{DR} too high by 0.2 dB) induces -15% on the estimated hourly rainfall accumulations and a bias of -0.2 dB (Z_{DR} too low by 0.2 dB) induces +15% on the

estimated hourly rainfall accumulations. An often mentioned requirement expressed by hydrologists with respect to radar QPE is to have a quantitative precipitation estimation that has – compared to rain gauges - no bias and a standard deviation error less than 20%. This sets a very demanding criterion on the calibration and stability of Z_{DR}.

The sensitivity of the conventional estimator (CONV) and the attenuation-corrected conventional estimator (CONV_ATT_BY_PDP) with respect to biases on Z_H is straightforward to compute (with the $Z=282R^{1.66}$ relationship used in this study): a bias of ±1 dB in Z_H – a typical precision that can be obtained and guaranteed by modern radars – leads to ±14% error (same sign as the error on Z_H) on the estimated rain rate. The gauge adjustment scheme, provided that there is sufficient rain and that it is triggered, may be able to compensate for that bias, given that it impacts equally all pixels in the radar domain.

Table 2 Impact of a ±0.2 dB simulated bias on ZDR on the ZZDR scores

DATE YYYY-MM-DD	No bias on Z_{DR}		+ 0.2 dB bias on Z_{DR}		- 0.2 dB bias on Z_{DR}	
	NB	COR	NB	COR	NB	COR
2005-04-06	0.12	0.85	-0.10	0.84	0.57	0.82
2005-04-18	0.00	0.80	-0.03	0.75	-0.04	0.61
2005-04-24	0.10	0.89	-0.13	0.90	0.30	0.89
2005-04-26	-0.09	0.87	-0.31	0.87	0.28	0.89
2005-05-14	-0.12	0.82	-0.32	0.80	0.02	0.83
2005-06-23	0.05	0.81	-0.15	0.73	0.11	0.72
2005-06-26	-0.08	0.92	-0.20	0.93	0.14	0.90
2005-06-28	0.53	0.87	0.33	0.89	0.90	0.85
2005-06-30	0.16	0.73	-0.03	0.70	0.40	0.73
2005-07-04	-0.21	0.84	-0.34	0.85	0.02	0.81
2005-07-28	0.25	0.84	0.03	0.83	0.55	0.79
GLOBAL	0.00	0.85	-0.17	0.83	0.12	0.82

The impact of a Z_H bias on ZZDR_ATT_BY_PDP and ZPHI is a little more complex to assess as both algorithms use Z_H at two stages : first to compute the concentration parameter of the DSD (N_W) and secondly to convert each reflectivity value into rainfall rate. The relative error on the estimated rain rate is of the opposite sign of the bias on Z_H and is equal to +19% in case of a 1 dB negative bias on Z_H (radar too cold) and -19% in the case of a 1 dB positive

bias on Z_H (radar too hot). This relative error is slightly higher compared to the relative error obtained by simply using a Z-R relationship.

Regarding ZZDR_ATT_BY_PDP, the same perturbation analysis can be conducted out. For a ±1 dB bias on Z_H, the ZZDR_ATT_BY_PDP estimator leads to an error on the rain rate of ±23% (same sign as the calibration bias on Z_H), which makes it the most sensitive estimator of all with respect to a calibration bias on Z_H.

Those sensitivity analyses, combined with operational experience on what is reasonably operationally achievable in terms of accuracy and stability of polarimetric variables Z_H and Z_{DR} are essential to select the most appropriate rain rate estimator.

5.4. Results of an extended study on polarimetric QPE

Dataset

Data from the year 2010 is analysed. Five different radars from different regions and with different characteristics are used. They are considered to be representative of the entire radar network. The selection of events is performed objectively using three criteria. Firstly, the daily average ground temperature close to the radar must be high enough so that the radar beam was below the iso-0° at 60 km. A standard atmosphere temperature decrease of –6°/km is used to estimate the altitude of the iso-0°. Secondly, a significant amount of rain must be present in the vicinity of the radar. The amount of rain is determined by calculating the average daily rainfall accumulation of all the rain gauges within a 60 km radius area. Events with an average rainfall accumulation higher than 10 mm are considered. Finally, the radar must be operational for the entire precipitation event. Table 3 lists the 29 radar-event couples that result from the objective selection.

Table 3 Selected events and elevation angles used in the data analysis

Radar	Elev [°]	Date
Avesnes	1.0	12, 14 July 15, 16, 26 Aug 2010
Blaisy	1.0	21, 22 July, 15, 16, 23, 27 Aug 7 Sept 2010
Cherves	1.0	10 June, 14 July, 8 Sept 2010
Montancy	1.2	28, 29 July, 2, 5, 12, 14, 15, 16, 24, 27 Aug 2010
Trappes	1.5	3, 12, 14 July 15 Aug 2010

Evaluated algorithms

In summary, the 10 algorithms that have been included in the evaluation exercise are:

- The Marshall-Palmer $Z_h=200R^{1.6}$ relationship without attenuation correction;
- The Marshall-Palmer $Z_h=200R^{1.6}$ relationship with attenuation correction;
- The Fulton et al. (1998) $Z_h=300R^{1.4}$ relationship without attenuation correction;
- The Fulton et al. (1998) $Z_h=300R^{1.4}$ relationship with attenuation correction;
- The Illingworth and Thompson (2005) $Z\text{-}Z_{dr}$ algorithm without attenuation correction;
- The Illingworth and Thompson (2005) $Z\text{-}Z_{dr}$ algorithm with attenuation correction;
- The Beard and Chuang (1987) $R\text{-}K_{dp}$ $R=29.7K_{dp}^{0.85}$;
- The Brandes et al. (2002) $R\text{-}K_{dp}$ $R=33.8K_{dp}^{0.79}$;
- A hybrid $Z_h\text{-}K_{dp}$ algorithm with a 0.5 ° km^{-1} K_{dp} threshold;
- A hybrid $Z_h\text{-}K_{dp}$ algorithm with a 1 ° km^{-1} K_{dp} threshold;

The 10 Pol-QPE algorithms are evaluated offline on a number of selected [radar;day] couples. The Z_{dr} data of each [radar;day] couple are corrected using the last azimuth-dependent Z_{dr} bias curve (see Section 2.2) that could be computed, in order to mimic real-time operations.

Evaluation results

The results are stratified according to three thresholds on the rain gauge hourly accumulations: > 0.2 mm (all rainfall accumulations, hereafter referred to as AR), > 1 mm (moderate and high hourly accumulations, hereafter referred to as MR) and > 5 mm (intense hourly accumulations, hereafter referred to as IR). The global results obtained with the 10 algorithms are also represented in Figure 24 (Figs. 24a – 24j). The score obtained by each algorithm is displayed on each sub-Figure for the three hourly accumulation thresholds 0.2, 1 and 5 mm. Notice that the horizontal and vertical scales on Figs. 24a – 24i are logarithmic. As it can be seen in Fig. 24a MP without attenuation correction significantly underestimates the rainfall rate (NB=-0.32 for AR). The underestimation is logically more pronounced at IR (NB=-0.46). Comparison between Figs. 24a and 24c shows that Marshall-Palmer without attenuation correction and WSR88D without attenuation correction have more or less the same performances.

The application of the polarimetric attenuation correction greatly improves the results of all the indicators. The correlation score of the Marshall-Palmer estimator (Figs. 24a and 24b)

goes up from 0.79 to 0.84 (AR) and from 0.61 to 0.78 (IR) when attenuation correction is applied. Similarly, the normalized bias is reduced from -0.32 to -0.22 (AR) and from -0.46 to -0.29 (IR). The RMS is also significantly improved. WSR88D with attenuation correction appears to outperform Marshall-Palmer in terms of normalized bias.

The Z_h-Z_{dr} algorithm (Figs. 24e and 24f) obtains quite decent scores, especially when attenuation correction is activated: in that case, the normalized bias and correlation are equal to 0.01 and 0.80 (AR) and 0.03 and 0.69 (IR). The bias is better than that obtained by the WSR88D with attenuation correction, but the correlation is comparable. This may seem a bit disappointing considering that the latter only uses Z_h, however this result is probably to be related to weaknesses in the calibration and/or correction for attenuation of Z_{dr}. It is also relevant the fact that Z_{dr} is only used in moderate precipitation. It is remarkable that the RMS increases when correcting for attenuation. This could point to errors in the estimation of the differential attenuation.

The results obtained with the R=f(K_{dp}) retrievals (Figs. 24g and 24h) clearly show the effect of not considering the negative values of K_{dp}. Indeed, the lowest rainfall accumulations are significantly overestimated. The correlation, however, is much larger than what is achieved with the Z_h-R and Z_h-Z_{dr} algorithms and exceeds 0.8 whatever rainfall accumulation threshold is considered. Between the two K_{dp} algorithms studied, the Beard and Chang R=f(K_{dp}) obtains the better scores.

The results of the hybrid algorithms (ZK_{dp}) are provided in Figs. 24i and 24j. We recall here that the algorithm uses, at the 5' time step, attenuation-corrected Z_h corrected into rainfall rate using Marshall-Palmer below a pre-determined threshold on K_{dp} (0.5 or 1° km^{-1}) and the Beard and Chuang R=f(Kdp) algorithm above that threshold. Both ZK_{dp} estimators appear to have excellent results, by far the best ones among all 10 algorithms. They both lead to low bias and correlation coefficients above 0.8 for all hourly rainfall accumulation thresholds (0.2, 1 and 5 mm). The RMS at IR is also the lowest and the Nash is the closest to one.

Figure 25 provides the variability of the AR (hourly rainfall accumulation above 0.2 mm) scores according to the 5 radars considered in this study. Figure 25a shows that Marshall-Palmer without attenuation correction underestimates precipitation for all radars except one. The improvement, in terms of bias and correlation, brought by attenuation correction on the Marshall-Palmer and WSR88D estimators is clearly visible on all radars. Z_h-Z_{dr} with attenuation correction leads to an overestimation for (almost) all radars. Interestingly, the variation between radars of the normalized bias and correlation is small. On the other hand,

ZK_{dp} algorithms (Figs. 25i and 25j) yield a larger variation of the scores between radars. The correlation coefficient is always high.

Figure 26 presents a stratification of the normalised bias according to the hourly rain gauge rainfall accumulation. Four classes of hourly precipitation accumulation have been selected: 0.2 – 1, 1 – 5, 5 – 10 and > 10 mm. The overall tendency of all algorithms is to overestimate the weakest hourly rainfall accumulations (0.2 – 1 mm) and underestimate the most intense ones (> 10 mm). This tendency is particularly pronounced for Marshall-Palmer without attenuation correction, WSR88D without attenuation correction and Z_h-Z_{dr} without attenuation correction. Even Marshall-Palmer with attenuation correction shows that behaviour. Z_h-Z_{dr} with attenuation correction and WSR88D with attenuation correction have both a normalized bias that is remarkably stable beyond the first class of hourly rainfall accumulation (above 1 mm), close to 0 (Z_h-Z_{dr} with attenuation correction) or negative (WSRD88D with attenuation correction). The ZK_{dp} normalised bias curve has a “U” shape, with the lowest hourly rainfall accumulations being overestimated (NB=0.25), the medium ones (1 – 10 mm) being slightly underestimated (NB=-0.15) and the highest ones (> 10 mm) being slightly overestimated (NB=+0.06). The larger overestimation of the lowest hourly rainfall accumulation of the ZK_{dp} algorithm respect to the attenuation corrected Marshall-Palmer is due to the influence of the R-K_{dp} retrieval on the hourly measurement. The R-K_{dp} retrieval is activated when instantaneous rainfall rate is higher than 16 mm/h (K_{dp} threshold at 0.5°) or 30 mm/h (Kdp threshold at 1.0°) approximately and at these rain rates it largely overestimates precipitation. Overall, ZK_{dp} with a threshold at 1° km^{-1} seems to be the best compromise.

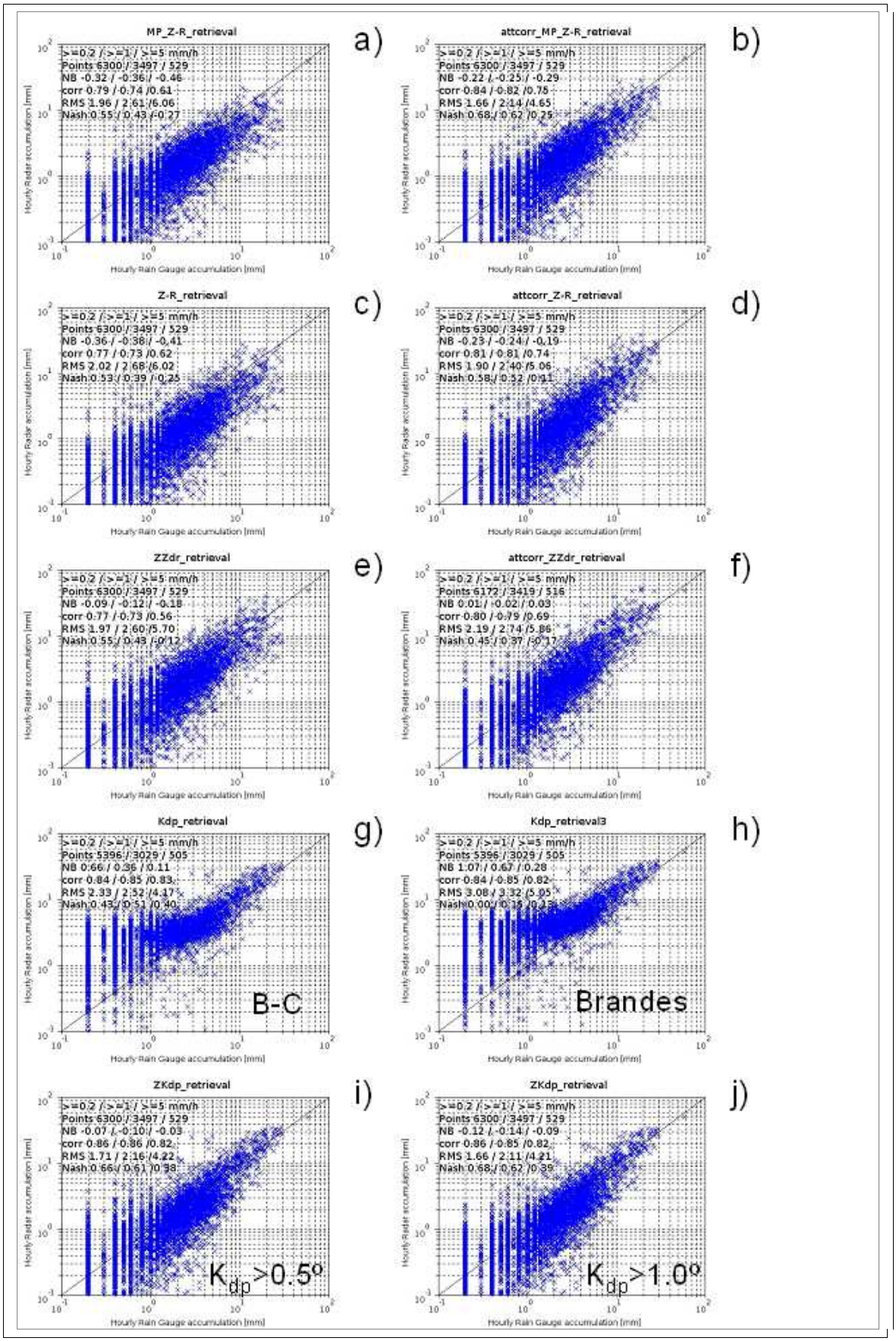

Figure 24 QPE results

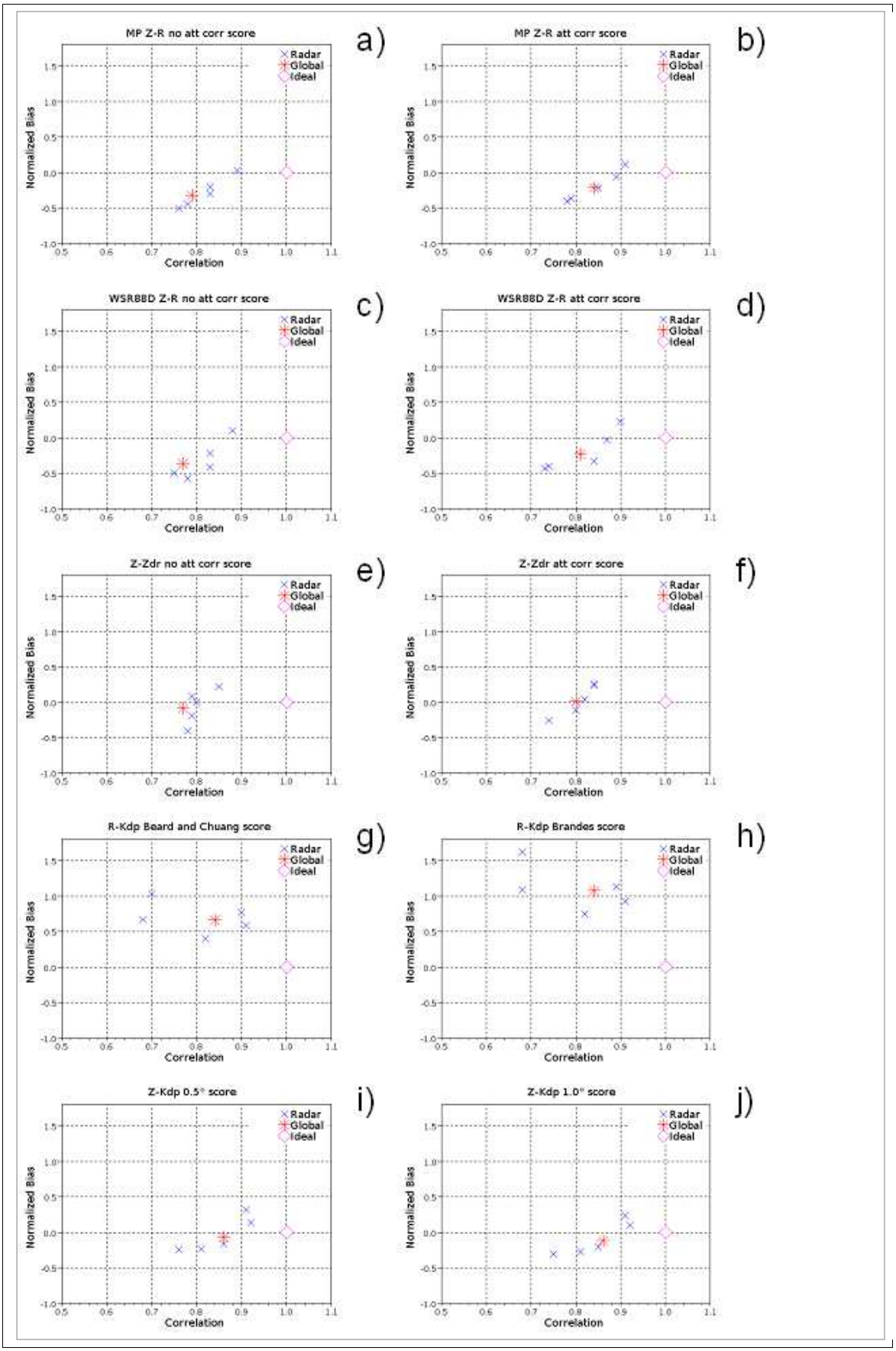

Figure 25 Results stratified by radar

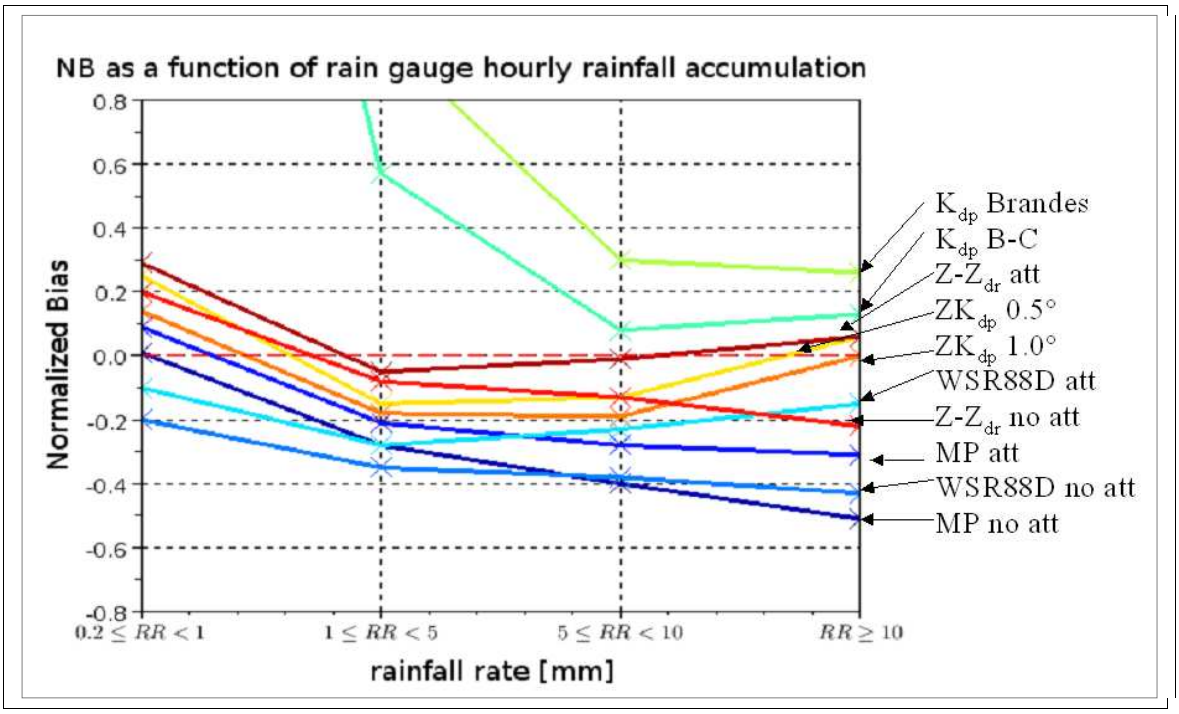

Figure 26 Results stratified by hourly rainfall accumulation

6. Conclusion

After several decades of research, polarimetric technology has now reached a sufficiently mature status to be introduced in the operational network of the weather services. In the last years, several services across Europe have started to use polarimetric radars. The report has provided an overview of these early experiences.

There is a wide consensus that polarimetry greatly improves the radar measurements quality. At the same time, a careful monitoring of the polarimetric variables is paramount to assess the radar data quality and for the early detection of hardware failures. All the services responsible for this report have implemented monitoring techniques aimed at assessing biases in Z_{dr}, the system Φ_{dp} offset and ρ_{hv} in rain and its evolution in time. These parameters seem to be a good indicator of the overall state of the radar system. The techniques to assess these biases are mainly based on vertically pointing scans and the use of sun hits. Long term measurements performed by Météo France show that, provided there are no changes in the hardware, those parameters are fairly stable. It has been signalled though, a fluctuation on the Z_{dr} bias which is likely to be dependent on the receiver temperature. Hence, the need for a good temperature control of the receiver. Experience by all services show that there is a spatial variation of Z_{dr} and the system Φ_{dp} offset that has to be accounted for. This spatial variation is mainly caused by the radome and nearby obstacles. Although , the use of random

panel designed radomes may minimize that effect it seems clear that it has nevertheless to be monitored.

The use of polarimetry requires a complex data processing in order to take full advantage of the microphysical information contained in the polarimetric variables. Météo France has developed an in-house polarimetric processing chain. The main functionalities of the chain are the clutter and artefact identification, the biases correction and the precipitation-induced attenuation correction, which is more and more relevant when the radar frequency is increased.

Polarimetry, has shown a great potential in decreasing the error in quantitative precipitation estimation. Météo France has performed several studies to assess the performance of various polarimetric QPE algorithms evaluating them against hourly rainfall accumulation from rain gauges. The results show a dramatic improve in the correlation and normalised bias of radar data respect to collocated rain gauges when polarimetric variables are used. From the studies it is concluded that given the current (insufficient) capacity to estimate biases in Z_{dr} accurately, the best algorithms are those based on K_{dp}, since such parameter is not sensitive to system miss-calibration or effects of Partial Beam Blocking on the data.

Given the initial experiences by the different weather radar services it seems now clear that polarimetry is indeed highly beneficial for operational radar networks and it will become the standard in Europe in the near future. Still, efforts have to be placed in improving the stability of the radar systems and optimising the data processing. Aside of the benefits of polarimetry in areas such as data quality monitoring, precipitation detection and quantitative precipitation estimation it has also the potential to provide other useful microphysics parameters such as hydrometeor type and the drop size distribution.

References

Beard KV, Chuang C. 1987. A New Model for the Equilibrium Shape of Raindrops. *J. Atmos. Sci.* 44: 1509-1524.

Brandes EA, Zhang G, Vivekanandan J. 2002. Experiments in Rainfall Estimation with a Polarimetric Radar in a Subtropical Environment. *J. Appl. Meteor.* 41: 674-685.

Bringi VN, Chandrasekar V. 2001. *Polarimetric Doppler Weather Radar*. Cambridge University Press: Cambridge.

Ciach GJ. 2003. Local Random Errors in Tipping-Bucket Rain Gauge Measurements. *J. Atmos. Oceanic*

Technol. 20: 752-759.

Delrieu G., Creutin JD, Andrieu H. 1995. Simulation of radar mountain returns using a digitized terrain model. *J. Atmos. Oceanic Technol*. 12: 1038-1049.

Emmanuel I, Andrieu H, Tabary P. 2011. Evaluation of the new French operational weather radar product for the field of urban hydrology. *J. Atmos. Research.* In press.

Frech, M., B. Lange, T. Mammen, J. Selt,mann, C Morehead and J. Rowan. 2012. Onsite radome performance verification. Submitted to *J. Atmos. Oceanic Technol*.

Fulton RA, Bredienbach JP, Seo D-J, Miller DA, O'Bannon T. 1998. The WSR-88 rainfall algorithm. *Wea. Forecasting.* 13: 377-395.

Gorgucci E, Scarchilli G, Chandrasekar V. 1994. A robust Estimator of Rainfall Rate Using Differential Reflectivity. *J. Atmos. Oceanic Technol*. 11: 586-592.

Gorgucci E, Scarchilli G, Chandrasekar V. 1999. Specific Differential Phase Estimation in the Presence of Nonuniform Rainfall Medium along the Path. *J. Atmos. Oceanic Technol.* 16: 1690-1697.

Gourley JJ, Tabary P, Parent du Chatelet J. 2006. Data Quality of the Meteo-France C-band Polarimetric Radar. *J. Atmos. Oceanic Technol*. 23: 1340-1356.

Gourley JJ, Tabary P, Parent du Chatelet J. 2007a: A Fuzzy Logic Algorithm for the Separation of Precipitating from Nonprecipitating Echoes Using Polarimetric Radar Observations. *J. Atmos. Oceanic Technol*. 24: 1439-1451.

Gourley JJ, Tabary P, Parent du Chatelet J. 2007b: Empirical Estimation of Attenuation from Differerential Propagation Phase Measurements at C Band. *J. Appl. Meteor. Climatol.* 46: 306-317.

Gourley JJ, Illingworth AJ, Tabary P. 2009. Absolute calibration of radar reflectivity using redundancy of the polarization observations and implied constraints on drop shapes. *J. Atmos. Oceanic Technol.* 26: 689-703.

Hitschfeld W, Bordan J. 1954. Errors inherent in the radar measurement of rainfall at attenuating wavelengths. *J. Meteor.* 11: 58-67.

Hogan R. 2007. A Variational Scheme for Retrieving Rainfall Rate and Hail Reflectivity Fraction from Polarization Radar. *J. Appl. Meteor. Climatol.* 46: 1544-1564.

Holleman I, Huuskonen A, Gill R, Tabary P. 2010. Operational Monitoring of Radar Differential Reflectivity Using the Sun. *J. Atmos. Oceanic Technol.* 27: 881-887.

Hubbert J, Bringi VN. 1995. An Iterative Filtering Technique for the Analysis of Copolar Differential Phase and Dual-Frequency Radar Measurements. *J. Atmos. Oceanic Technol.* 12: 643-648.

Hubbert JC, Ellis SM, Dixon M, Meymaris G. 2010. Modeling, Error Analysis, and Evaluation of Dual-Polarization Variables Obtained from Simultaneous Horizontal and Vertical Polarization Transmit Radar. Part I: Modeling and Antenna Errors. *J. Atmos. Oceanic Technol.* 27: 1583-1598.

Illingworth AJ, Thompson RJ. 2005. 'The Estimation of Moderate Rain Rates with Operational Polarisation Radar'. In *Proceedings of 32nd Conference on Radar Meteorology, Albuquerque, NM, 24-29 Oct. 2005.* American Meteorological Society: Boston, MA.

Le Bouar, E., Testud J, Keenan T. 2001. Validation of the Rain Profiling Algorithm "ZPHI" from the C-Band Polarimetric Weather Radar in Darwin, *J. Atmos. Oceanic Technol.* 18: 1819–1837.

Marshall JS, Langille RC, Palmer WK. 1947. Measurement of Rainfall by Radar. *J. of Meteorology,* 4: 186-192.

Mudukutore A, Chandrasekar V, Mueller EA. 1995. The Differential Phase Pattern of the CSU CHILL Radar Antenna. *J. Atmos. Oceanic Technol.* 12 : 1120 - 1123.

Parent-du-Châtelet J, Perier L, do Khack K, Roquain P. 2001. 'CASTOR2, a new computer for the French radar network'. In *Proceedings of 32nd Conference on Radar Meteorology, Munich, Germany, 18-24 July 2001.* American Meteorological Society: Boston, MA.

Ryzhkov A, Zrnic D. 1996. Assessment of Rainfall Measurement that Uses Specific Differential Phase. *J. Appl. Meteor.* 35: 2080-2090.

Ryzhkov A, Giangrande SE, Schuur TJ. 2005. Rainfall Estimation with a Polarimetric Prototype of WSR-88D. *J. Appl. Meteor.* 44: 502-515.

Sachidananda M, Zrnic D. 1987. Rain Rate Estimates from Differential Polarization Measurements. *J. Atmos. Oceanic Technol.* 4 : 588-598.

Sugier J, Parent-du-Châtelet J, Roquain P, Smith A. 2002. 'Detection and removal of clutter and anaprop in radar data using a statistical scheme based on echo fluctuation'. In Proceedings of 2nd European Radar *European Conference on Radar in Meteorology and Hydrology, Delft, The Netherlands, 18–22 Nov. 2002.*

Sugier, J, Tabary P. 2006. *Evaluation of dual-polarization technology at C-band for operational weather radar network.* Report of the EUMETNET Opera 2, Work packages 1.4 and 1.5, Deliverable b [available at www.knmi.nl/opera], 44 pp.

Tabary P, Le Henaff G, Vulpiani G, Parent-du-Châtelet J, Gourley JJ. 2006. 'Melting layer characterization and identification with a C-band dual-polarization radar: A long-term analysis'. In *Proceedings of 4th European Conference on Radar in Meteorology and Hydrology, Barcelona, Spain, 18-22 Sept. 2006.* Servei Meteorològic

de Catalunya: Barcelona.

Tabary P. 2007. The New French Operational Radar Rainfall Product. Part I: Methodology. *Wea. Forecasting*. 22: 393-408.

Tabary P, Le Henaff G, Dupuy P, Parent-du Châtelet J, Testud J. 2008. 'Can we use polarimetric X-band radars for operational quantitative precipitation estimation in heavy rain regions?', In *Proceedings of Weather Radar and Hydrology International Symposium, Grenoble, France, 10-15 March 2008.*

Tabary P, Berthet C, Dupuy P, Figueras i Ventura J., Fradon B, Georgis JF, Hogan R, Kabeche F, Wasselin JP. 2010. 'Hail detection and quantification with C-band polarimetric radars: results from a two-year objective comparison against hailpads in the south of France'. In *Proceedings of 6th European Conference on Radar in Meteorology and Hydrology, Sibiu, Romania, 6-10 Sept. 2010.*

Tabary P, Boumahmoud A-A, Andrieu H, Thompson RJ, Illingworth AJ, Le Bouar E, Testud J. 2011. Evaluation of two "integrated" polarimetric Quantitative Precipitation Estimation (QPE) algorithms at C-band. *J. of Hydrology*. In press.

Testud J, Le Bouar E, Obligis E, Ali-Mehenni M. 2000. The Rain Profiling Algorithm Applied to Polarimetric Weather Radar. . *J. Atmos. Oceanic Technol.* 17: 332-356.

Tuttle JD, Foote GB. 1990. Determination of boundary layer airflow from a single Doppler radar. *J. Atmos. Oceanic Technol*. 7: 218-232.

Vulpiani G, Giangrande S, Marzano FS. 2009. Rainfall Estimation from Polarimetric S-Band Radar Measurements: Validation of a Neural Network Approach. *J. Appl. Meteor. Climatol*. 48: 2022-2036.

Wang Y, Chandrasekar V. 2009. Algorithm for Estimation of the Specific Differential Phase. *J. Atmos. Oceanic Technol*. 26: 2565-2578.

Zrnic D, Doviak R, Zhang G, Ryzhkov A. 2010. Bias in differential reflectivity bias due to cross coupling through the radiation patterns of polarimetric weather radars, *J. Atmos. Oceanic Technol.* 27: 1624-1637.